Supplementary information for

A Water-soluble, Cell-permeable Mn(II) Sensor Enables Visualization of Manganese Dynamics in Live Mammalian Cells

Smitaroopa Kahali,[1‡] Sujit Kumar Das,[1‡] Ravinder Kumar,[1] Kunika Gupta,[1] Rajasree Kundu,[1] Baivabi Bhattacharya,[2] Arnab Nath,[2] Ravindra Venkatramani [1] and Ankona Datta[*1]

[1]Department of Chemical Sciences, Tata Institute of Fundamental Research, Mumbai, 400005, India

[2]Department of Developmental Biology and Genetics, Indian Institute of Science, Bangalore, 560012, India

[‡]Equal Contribution

[*]Corresponding author: Ankona Datta

Email: ankona@tifr.res.in

General Procedures and Methods

All chemicals used were of analytical grade, obtained from commercial sources and used without further purification. Chemicals were purchased from either Sigma Aldrich®, or SD Fine-Chem Ltd., or TCI India Research Chemicals, or Alfa Aesar, or Arrobiochem Private limited and used without further purification unless otherwise noted. All cell culture reagents were purchased from either Sigma Aldrich® or Gibco®. Methanol, dichloromethane (DCM), and *N,N*-dimethylformamide (DMF) were dried using activated molecular sieves. Tetrahydrofuran (THF) was distilled and degassed thoroughly by purging argon (Ar) before using in detosylation reaction. All experiments were performed in deionized water taken from a Milli-Q® Integral 3 water purification unit (Millipore Corp. Billerica, MA, USA). Silica gel (200-400 mesh size, Loba Chemie Pvt. Ltd.) and alumina (70-230 mesh size, Loba Chemie Pvt. Ltd.) were used for column chromatography. Compounds eluted from column chromatography purifications were characterized by thin layer chromatography (TLC) analysis. TLC analyses were performed on silica gel 60 F_{254} (Merck & Co., Inc.) and aluminum oxide 60 F_{254} (Merck & Co., Inc.) TLC plates and the plates were visualized under UV light, 254 nm and 365 nm. Analytical grade solvents were used for separation and used without distillation. Solvents were evaporated under reduced pressure using a rotary evaporator (BÜCHI Labortechnik AG).

^{1}H NMR and ^{13}C NMR spectra were collected in either $CDCl_3$ or CD_3OD as a solvent (Cambridge Isotope Laboratories, Cambridge, MA) at 25 °C on either a Varian 600 MHz spectrometer or Bruker 800 MHz spectrometer at the National NMR facility, Tata Institute of Fundamental Research, Mumbai, India or Bruker 400 MHz spectrometer at the Indian Institute of Technology, Bombay, Mumbai, India. All chemical shifts are reported in the standard notation of parts per million (ppm) using the peaks of proton signals of residual solvents for calibration. The abbreviations used for the proton spectra multiplicities are: s, singlet; br, broad singlet; d, doublet; t, triplet; m, multiplet.

HEK 293T and HeLa cells were purchased from American Type Culture Collection (ATCC®).

UV-Visible spectrophotometric experiments were performed on a Thermo Scientific Multiskan Go spectrophotometer in a quartz cuvette having a path length of 1 cm with 10 mm x 4 mm (Hellma® Analytics) inner dimensions.

Liquid chromatography mass spectrometry (LCMS) analyses were carried out on a Shimadzu LCMS 2020 with an electrospray ionization (ESI) probe (positive and negative ion modes). High-resolution

mass spectrometry (HRMS) analyses were carried out either at the Chemistry Department, Indian Institute of Technology, Bombay, India on a maXisTM impact ESI-qTOF mass spectrometer (Bruker Corp.) or at the HRMS facility at the Indian Institute of Science Education and Research, Pune, India. For cell viability experiments, a Biotech Cytation 5 Analyzer microplate reader was used for measuring absorbance at 570 nm in a 96 well plate.

Table S1. Results from the TD-DFT calculations on **M1**, **M'**, **M"**, **M3** and **M4**. Based on the absorption wavelength (closest to expected, based on BODIPY absorption) and the oscillator strength (f) values, the most probable vertical transitions have been highlighted in red. Transitions with the maximum oscillator strength were considered as the most probable transition in each case.

M1			
Transition	**Transition Wavelength**	**Oscillator Strength (f)**	**MO Contributions**
HOMO-1 -> LUMO	**421**	**0.0006**	**0.70**
HOMO-2 -> LUMO	**431**	**0.5518**	**0.69**
HOMO-6-> LUMO			**0.11**
HOMO-1 -> LUMO	**460**	**0.0000**	**0.71**
M'			
HOMO-> LUMO	**415**	**0.7371**	**0.69**
M"			
HOMO-> LUMO	**512**	**1.1840**	**0.67**
M3			
HOMO-2-> LUMO	**439**	**0.4234**	**0.61**
HOMO-1 -> LUMO			**0.23**
HOMO -> LUMO			**0.17**
M4			
HOMO-4 -> LUMO	**407**	**0.0003**	**0.71**
HOMO-3 -> LUMO	**438**	**0.0007**	**0.71**
HOMO-2 -> LUMO	**443**	**0.5558**	**0.68**
HOMO-6 -> LUMO			**0.12**
HOMO-1 -> LUMO	**465**	**0.0007**	**0.69**
HOMO-2 -> LUMO			**0.14**

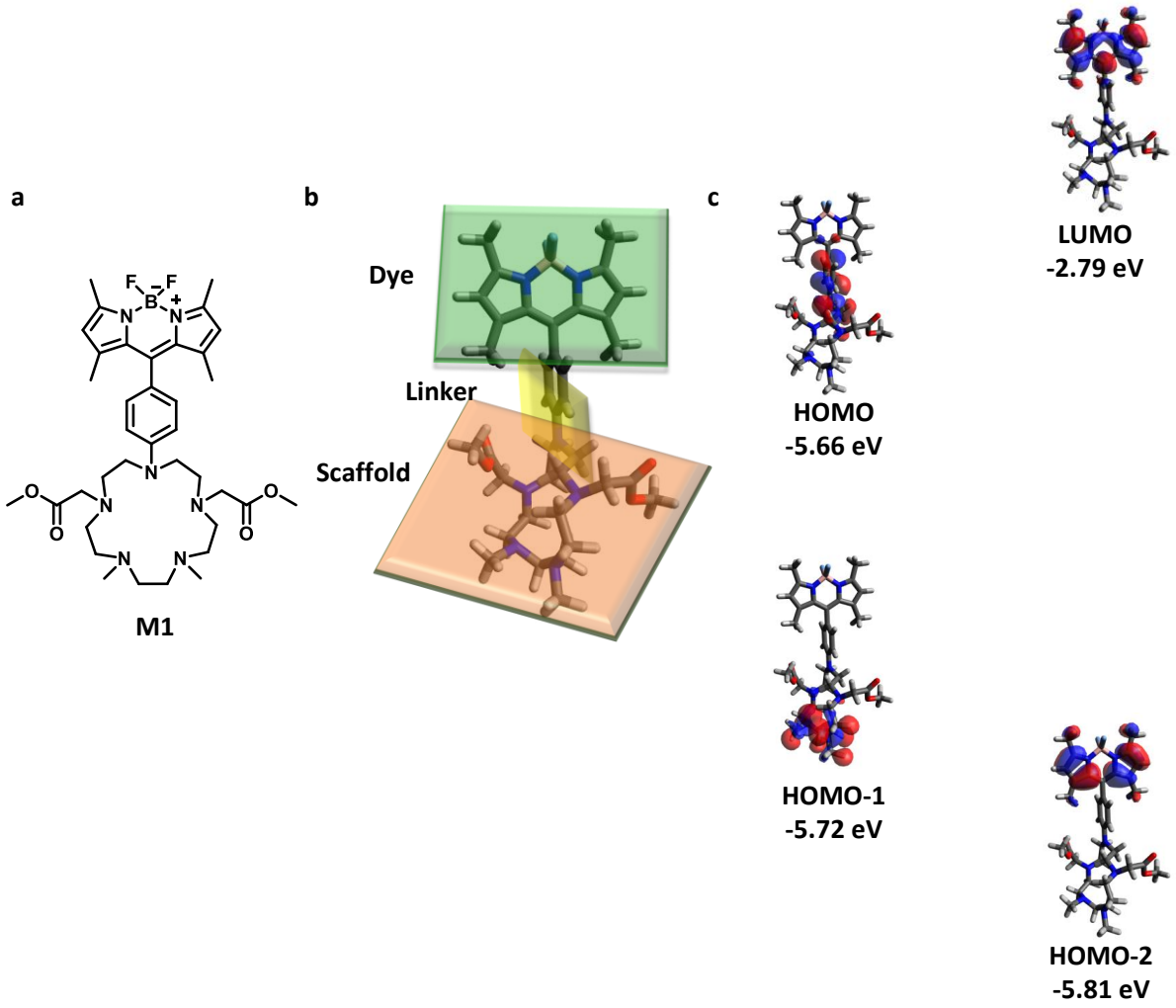

Figure S1. (a) Chemical structure of **M1**. (b) Optimized geometry of **M1** in ACN (DFT geometry optimization using B3LYP and 6-311++G**). The three parts of the molecule (the dye, the linker, and the scaffold) are at different planes marked in green, yellow, and orange respectively. (c) Orbitals of **M1** showing distinct localization on either the dye or the scaffold part of the molecule. Energy levels are not drawn to scale.

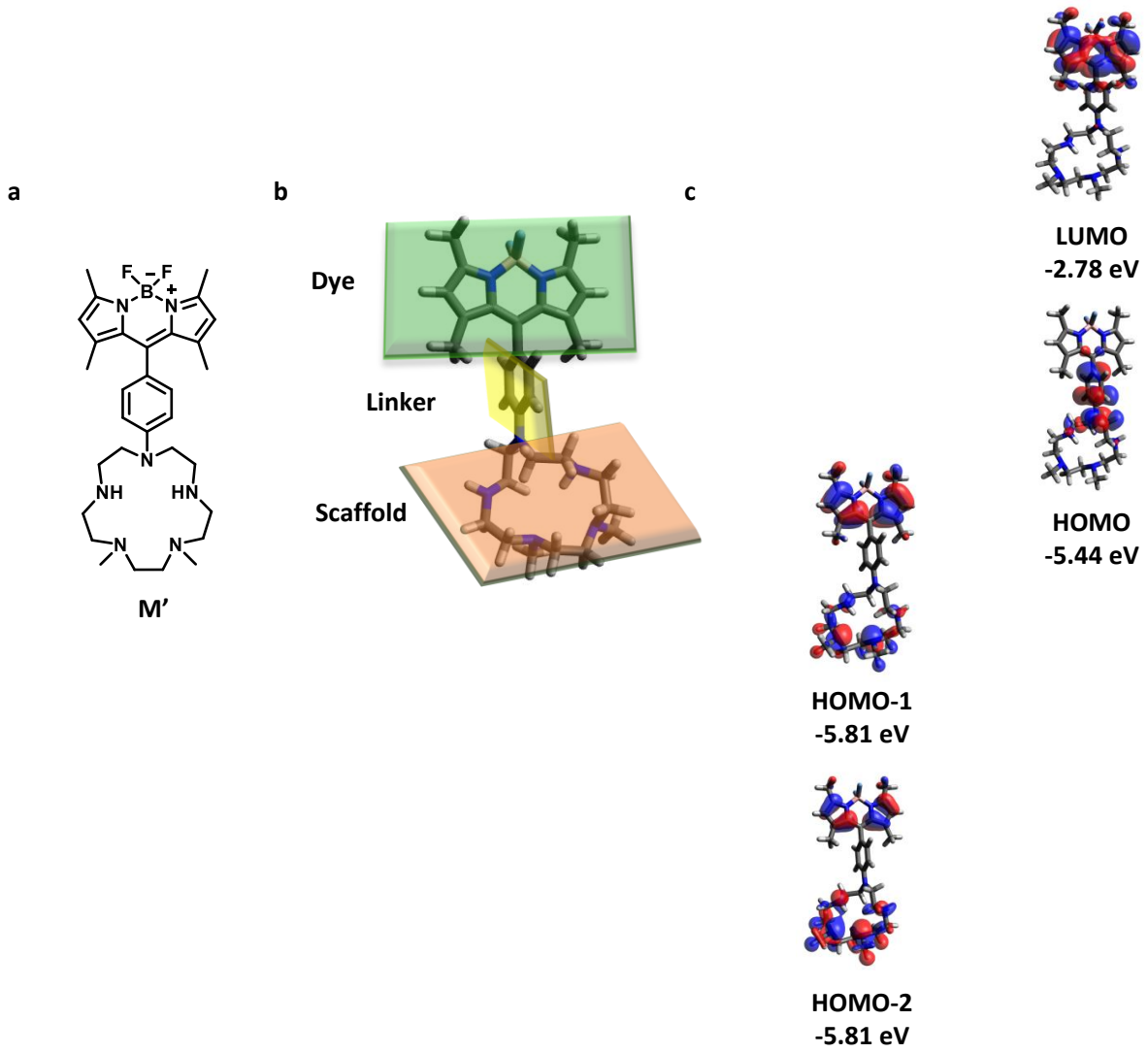

Figure S2. (a) Chemical structure of **M'**. (b) Optimized geometry of **M'** in water (DFT geometry optimization using B3LYP and 6-311++G**). The three parts of the molecule (the dye, the linker, and the scaffold) are at different planes marked in green, yellow, and orange respectively. (c) Orbitals of **M'**. Energy levels are not drawn to scale.

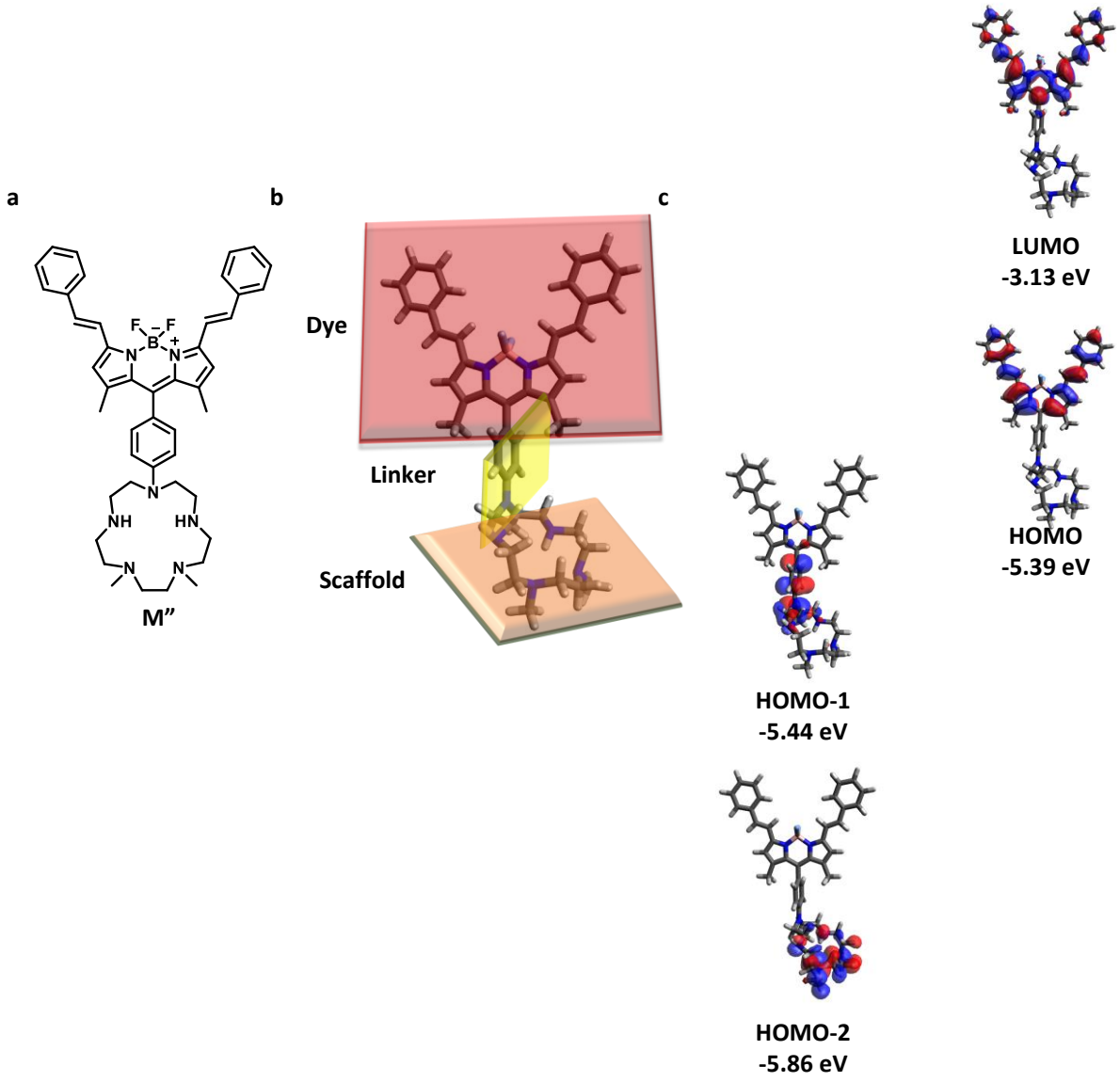

Figure S3. (a) Chemical structure of **M”**. (b) Optimized geometry of **M”** in water (DFT geometry optimization using B3LYP and 6-311++G**). The three parts of the molecule (the dye, the linker, and the scaffold) are at different planes marked in red, yellow, and orange respectively. (c) Orbitals of **M”** showing distinct localization on either the dye or the scaffold part of the molecule. Energy levels are not drawn to scale.

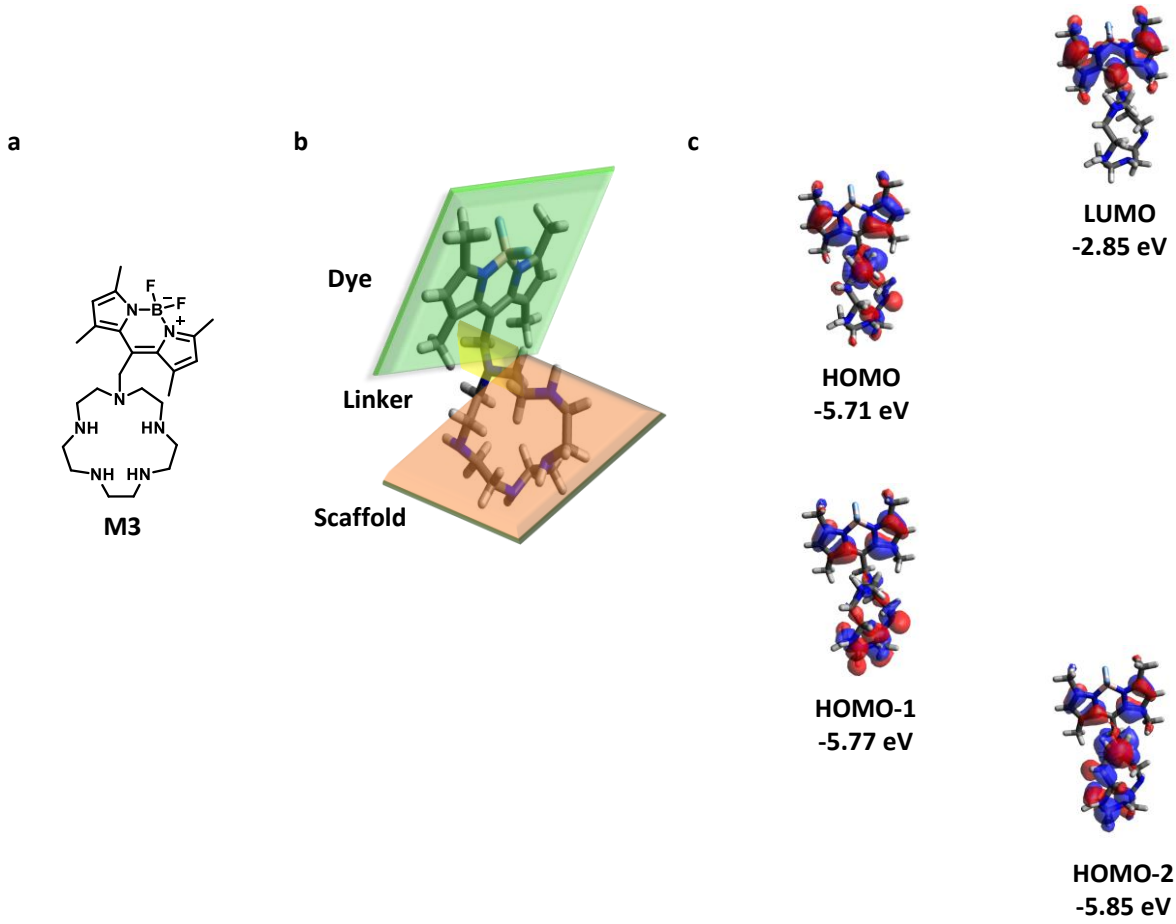

Figure S4. (a) Chemical structure of **M3**. (b) Optimized geometry of **M3** in water (DFT geometry optimization using B3LYP and 6-311++G**). The three parts of the molecule (the dye, the linker, and the scaffold) are at different planes marked in green, yellow, and orange respectively. (c) Orbitals of **M3**. Energy levels are not drawn to scale.

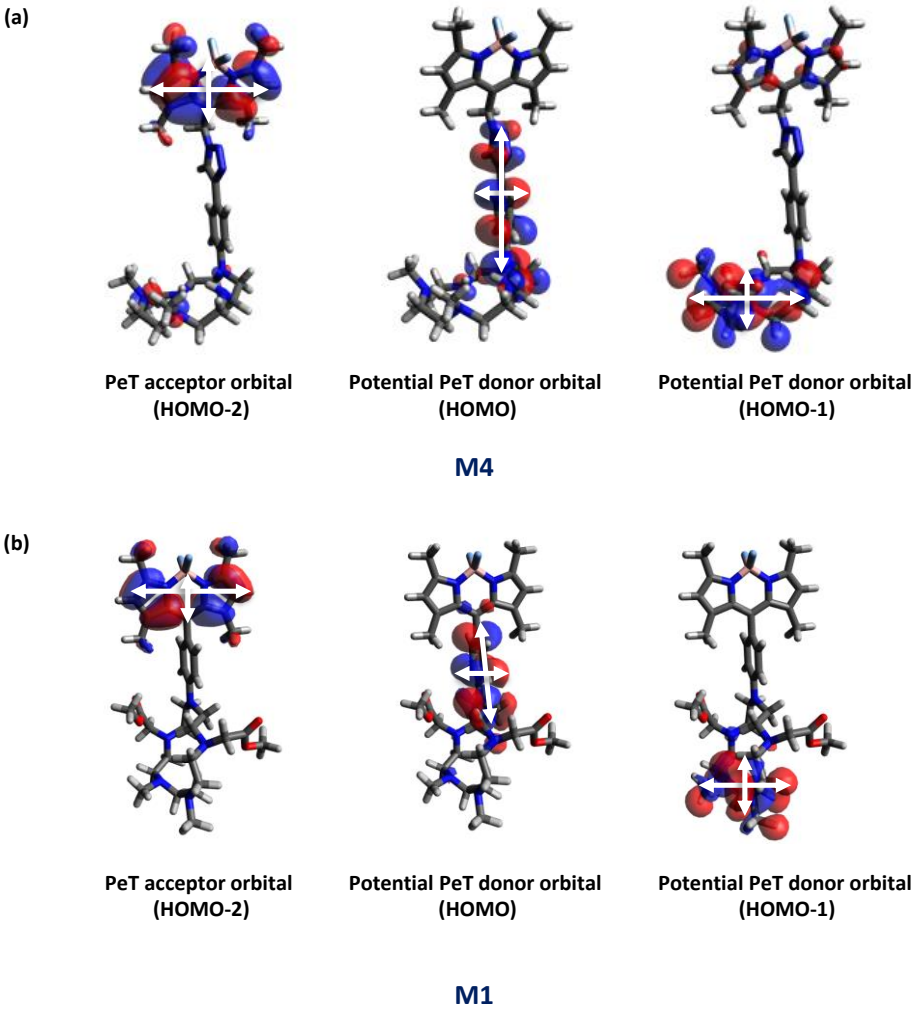

Figure S5. (a) Potential PeT donor and acceptor orbitals of **M4**. White arrows indicate the distance considered for calculating a_1 and a_2 for calculation of reorganization energy (λ_o). The average of horizontal and vertical arrows of the donor orbital was taken as $2a_1$ and the average of horizontal and vertical arrows of the acceptor orbital was taken as $2a_2$. (b) Potential PeT donor and acceptor orbitals of **M1**. White arrows indicate the distance considered for calculating a_1 and a_2 for calculation of reorganization energy (λ_o). The average of horizontal and vertical arrows of the donor orbital was taken as $2a_1$ and the average of horizontal and vertical arrows of the acceptor orbital was taken as $2a_2$.

Table S2. Calculated parameters relevant to the Rehm-Weller equation.

Molecule	Solvent	Donor Orbital	Acceptor Orbital	E_D (eV)	E_A (eV)	$\Delta E_{0,0}$ (eV)	W_P (eV)	ΔG (eV)
M4	Water	HOMO	HOMO-2	-5.43	-5.95	2.79	1.73×10^{-18}	-2.28
		HOMO-1	HOMO-2	-5.92	-5.95	2.79	1.26×10^{-18}	-2.77
M1	ACN	HOMO	HOMO-2	-5.66	-5.81	2.88	2.54×10^{-18}	-2.73
		HOMO-1	HOMO-2	-5.72	-5.81	2.88	1.19×10^{-18}	-2.78

Table S3. Parameters relevant to the calculation of λ_o.

Molecule	Solvent	Donor Orbital	Acceptor Orbital	a_1 (Å)	a_2 (Å)	r (Å)	λ_o (eV)
M4	Water	HOMO	HOMO-2	6.76	6.46	8.51	1.48
		HOMO-1	HOMO-2	6.63	6.46	11.71	1.76
M1	ACN	HOMO	HOMO-2	5.03	6.45	5.81	1.39
		HOMO-1	HOMO-2	6.81	6.45	12.41	1.70

Table S4. Calculated free energy (ΔG), electronic coupling (H_{DA}), reorganization energy (λ), and rate for PeT.

Molecule	Solvent	Donor Orbital	Acceptor Orbital	ΔG (eV)	H_{DA} (eV)	λ (eV)	K_{et} (s^{-1})
M4	Water	HOMO	HOMO-2	-2.28	0.147	1.48	4.09×10^{12}
		HOMO-1	HOMO-2	-2.77	0.015	1.76	9.13×10^{9}
M1	ACN	HOMO	HOMO-2	-2.73	0.002	1.39	2.93×10^{5}
		HOMO-1	HOMO-2	-2.79	0.002	1.70	4.44×10^{7}

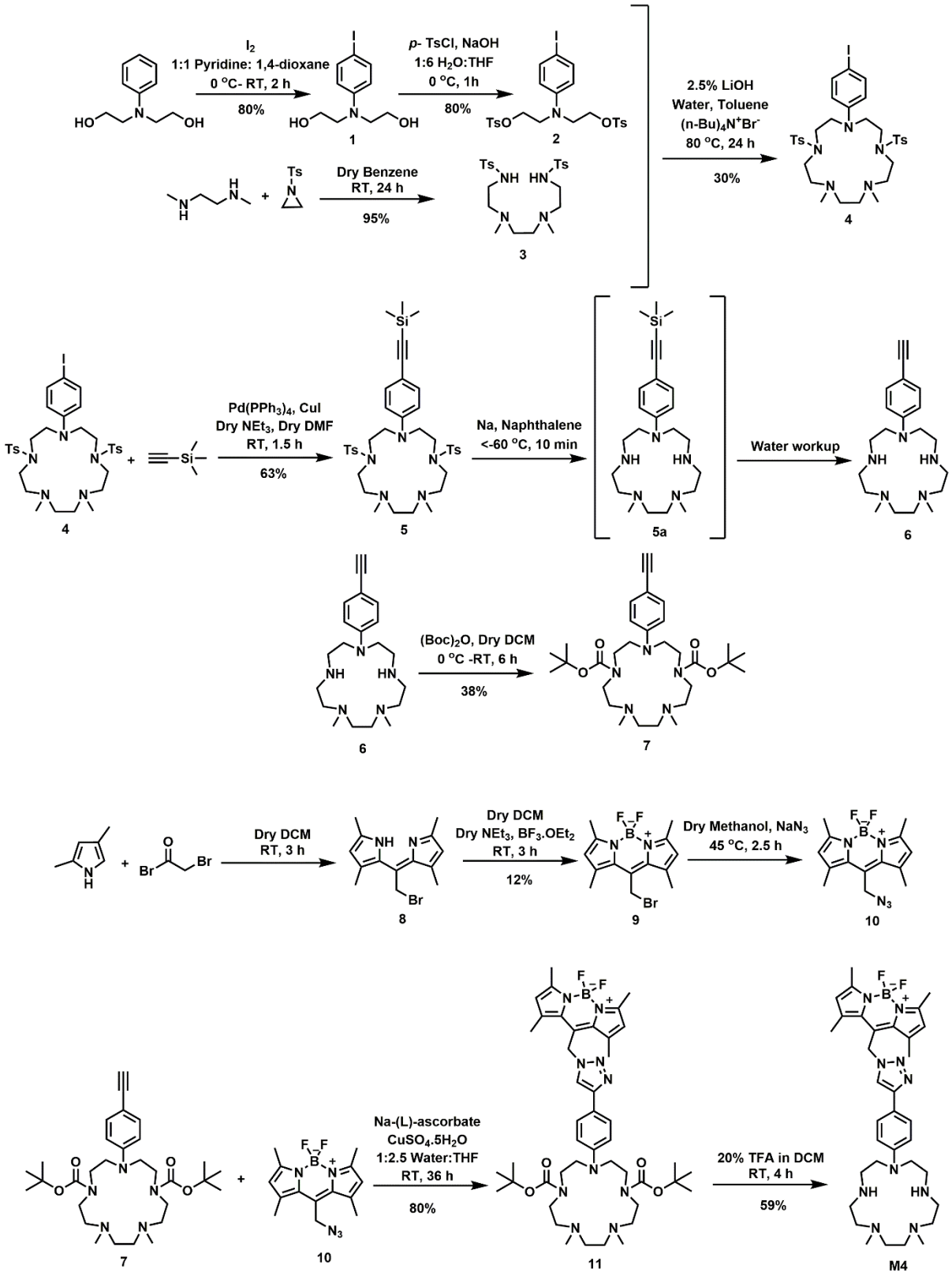

Figure S6. Synthetic scheme for **M4**.

Synthesis and Characterization of M4

2,2'-((4-iodophenyl)azanediyl)diethanol (1): Compound **1** was synthesized according to a previously reported procedure.[1]

((4-iodophenyl)azanediyl)bis(ethane-2,1-diyl) bis(4-methylbenzenesulfonate) (2):

A solution of sodium hydroxide (0.227 g, 5.68 mmol) in water (4 mL) and compound **1** (0.25 g, 0.81 mmol) in THF (12 mL) were taken in a round bottom flask and was kept in an ice bath. To that solution, *p*-toluene sulphonyl chloride (0.54 g, 2.84 mmol) dissolved in tetrahydrofuran (12 mL) was added slowly over a period of 20 min, keeping the temperature at 0 °C. The reaction mixture was then allowed to stir at 0 °C for 1 h. The reaction mixture was then poured into ice cold water (70 mL) to afford a white precipitate of compound **2** (0.39 g, 80 %).

It was noted that ratio of water and THF was a crucial parameter in the reaction.

^{1}H NMR (600 MHz, $CDCl_3$, 298 K): δ (ppm) 7.68 (4H, d, J= 7.8 Hz), 7.35 (2H, d, J= 9 Hz), 7.27 (4H, d, J= 8.2 Hz), 6.19 (2H, d, J= 9 Hz), 4.07 (4H, t, J= 6 Hz), 3.52 (4H, t, J= 6 Hz), 2.43 (6H, s).

^{13}C NMR (150 MHz, $CDCl_3$, 298 K): δ (ppm) 148.02, 147.76, 140.57, 132.51, 130.44, 116.0, 81.24, 68.84, 52.71, 32.32, 24.33.

LRMS (ESI): Calculated mass for $[M+H]^+$ $C_{24}H_{26}INO_6S_2$ 616, observed 616 and 638 corresponding to $[M+Na]^+$.

Compound **2** had already been reported and synthesized by a different procedure. All characterization data matched with the previously reported molecule.[2]

N,N'-((ethane-1,2-diylbis(methylazanediyl))bis(ethane-2,1-diyl))bis(4-methylbenzenesulfonamide) (3): Compound **3** was synthesized according to the previously reported procedure.[3]

1-(4-iodophenyl)-7,10-dimethyl-4,13-ditosyl-1,4,7,10,13-pentaazacyclopentadecane (4):

Tetrabutyl ammonium bromide (0.084 g, 0.26 mmol) was added to a mixture of lithium hydroxide in

water (2.5 %, 10 mL) and toluene (10 mL). The mixture was then refluxed at 80 ˚C for 30 min. In the reaction mixture, a slurry of compound **3** (0.25 g, 0.52 mmol) and **2** (0.32 g, 0.52 mmol) in toluene (10 mL) were added and the mixture was allowed to stir for 24 h, maintaining the temperature at 80 ˚C. After 24 h, the reaction mixture was cooled to room temperature and washed multiple times with water to remove tetrabutyl ammonium bromide from organic layer. The organic layer was then dried over anhydrous sodium sulphate and was concentrated under vacuum. The compound was purified by column chromatography (silica gel, 1% methanol in DCM) to afford compound **4** as a white crystalline solid (0.118 g, 30 %).

^{1}H NMR (600 MHz, $CDCl_3$, 298 K): δ (ppm) 7.66 (4H, d, J= 6 Hz), 7.52 (2H, d, J= 6 Hz)

7.29 (4H, d, J= 6 Hz), 6.75 (2H, d, J= 6 Hz), 3.73 (4H, t, J= 6 Hz), 3.20 (4H, t, J= 6 Hz), 3.06

(4H, t, J= 6 Hz), 2.54 (4H, t, J= 6 Hz), 2.44 (4H, s), 2.41 (6H, s), 2.16 (6H, s).

^{13}C NMR (150 MHz, $CDCl_3$, 298 K): δ (ppm) 147.18, 143.65, 138.25, 135.75, 129.98, 127.28, 114.04, 79.52, 60.87, 56.69, 50.60, 48.23, 47.03, 41.39, 21.64.

HRMS: Calculated mass for $[M+Na]^+$ $C_{32}H_{44}IN_5NaO_4S_2$ 776.1770, observed 776.1769, and calculated mass for $[M+H]^+$ 754.1958, observed 754.1992.

1,4-dimethyl-7,13-ditosyl-10-(4-((trimethylsilyl)ethynyl)phenyl)-1,4,7,10,13-pentaazacyclopentadecane (5): Copper iodide (0.002 g, 0.01 mmol) was added to a three-neck dried round bottom flask charged with nitrogen. Tetrakistriphenyl phosphine palladium (0) (0.023 g, 0.019 mmol) in dry DMF (3 mL) was added into the reaction mixture. The solution was then stirred for 5 min. Compound **4** (0.09 g, 0.1234 mmol) in dry DMF (5 mL) was added into the reaction mixture followed by the addition of triethylamine (0.171 mL, 1.23 mmol). The reaction mixture was then allowed to stir at room temperature for 10 min. Trimethylsilylacetylene (0.036 mL, 0.26 mmol) in dry DMF (2 mL) was then added slowly into the reaction mixture over a period of 5 min. The reaction mixture was stirred at room temperature for 1.5 h. The mixture was then added into excess DCM and

washed several times with water (4 x 50 mL). The organic phase was dried over anhydrous sodium sulphate and concentrated under vacuum. The compound was purified by column chromatography (silica gel, 0.8% Methanol in DCM) to obtain compound **5** as yellow solid (0.054 g, 63 %). We noted that addition order of the reagents was important. The completion of the reaction was confirmed by appearance of a dark brown color. The reaction was stopped immediately after the color changed to dark brown and it was observed that letting the reaction continue for longer times could affect the yield.

^{1}H NMR (600 MHz, $CDCl_3$, 298 K): δ (ppm) 7.66 (4H, d, *J*= 6 Hz), 7.40 (2H, d, *J*= 6 Hz), 7.29 (4H, d, *J*= 6 Hz), 6.85 (2H, d, *J*= 6 Hz), 3.77 (4H, t, *J*= 6Hz), 3.21 (4H, br), 3.05 (4H, t, *J*= 6 Hz), 2.56 (4H, br), 2.44 (4H, s), 2.41 (6H, s), 2.16 (6H, s), 0.25 (9H, s).

^{13}C NMR (200 MHz, $CDCl_3$, 298 K): δ (ppm) 143.70, 135.51, 133.82, 129.99, 127.29, 123.65, 114.21, 111.12, 106.73, 91.32, 60.84, 56.80, 48.31, 47.16, 41.38, 32.06, 21.64, 0.39.

HRMS: Calculated mass for $[M+H]^+$ $C_{37}H_{54}N_5O_4S_2Si$ 724.3406, observed 724.3406.

10-(4-ethynylphenyl)-1,4-dimethyl-1,4,7,10,13-pentaazacyclopentadecane (6): Sodium metal (0.5 g) and naphthalene (0.15 g, 1.15 mmol) were added to dry THF under argon. The mixture was sonicated for 15 min to yield a green-coloured solution of sodium naphthalenide and it was cooled to -78 ˚C (attained by adding dry ice in acetone). A solution of compound **5** (0.025 g, 0.034 mmol) in dry THF (5 mL) was added to the cooled solution of sodium naphthalenide and the mixture was then stirred for 10 min, maintaining the temperature at < -60 ˚C. The reaction was quenched by carefully adding it in portions into water (50 mL). The reaction mixture was added to excess water, in this case 50 mL, to ensure complete desilylation of the intermediate **5a**. Water was then evaporated, and the residue was dissolved in methanol. The mixture was filtered through a 0.2 µM filter to remove salts and was evaporated to dryness. Finally, the residue was re-dissolved in DCM to remove the dissolved salts in methanol. The crude product was taken forward to the next step without further purification.

LRMS (ESI): Calculated mass for $[M+H]^+$ $C_{20}H_{34}N_5$ 344, observed 344, and 366 = $[M+Na]^+$.

di-tert-butyl-4-(4-ethynylphenyl)-10,13-dimethyl-1,4,7,10,13-pentaazacyclopentadecane-1,7-dicarboxylate (7): Compound **6** (0.05 g, 0.15 mmol) was dissolved in dry DCM (20 mL) and added to a three-neck round bottom flask charged with argon. Triethylamine (0.05 mL, 0.36 mmol) in dry DCM (5 mL) was then added into the reaction mixture containing compound **6**. The mixture was then cooled to 0 ˚C. Ditertbutyl dicarbonate (0.071 mL, 0.33 mmol) in dry DCM (5 mL) was then slowly added into the reaction mixture keeping the temperature at 0 ˚C. Reaction mixture was then allowed to stir for another 6 h. Organic phase was dried under vacuum. The compound was purified by column chromatography (neutral alumina, 0.5% MeOH in DCM) to afford compound **7** as yellow sticky solid (0.03 g, 38 %).

^{1}H NMR (800 MHz, $CDCl_3$, 298 K): δ (ppm) 7.30 (1H, d, *J*= 8 Hz), 7.29 (1H, d, *J*= 8 Hz), 6.86 (1H, d, *J*= 8 Hz), 6.81 (1H, d, *J*= 8 Hz), 3.65-3.61 (4H, m, br), 3.40-3.34 (8H, m, br), 3.34-3.31 (4H, m), 2.97-2.96 (1H, s), 2.50 (4H, s, br), 2.45 (4H, s), 2.23 (6H, s), 1.57-1.55 (18 H, s, br).

^{13}C NMR (200 MHz, $CDCl_3$) δ 155.78, 155.58, 148.45, 133.56, 133.34, 111.47, 111.28, 108.38, 85.19, 84.96, 80.41, 79.71, 74.84, 74.64, 59.69, 59.55, 59.31, 56.19, 56.05, 55.94, 49.29, 48.98, 47.78, 47.33, 46.85, 45.93, 42.79, 42.38, 28.80, 28.64.

HRMS (ESI): Calculated mass for $[M+H]^+$ $C_{30}H_{50}N_5O_4$ 544.3936, observed 544.3943.

In the ^{1}H NMR of compound **7**, the number of peaks observed were more than expected (approximately a pair of signals at every ppm value). This might be attributable to the presence of two rotational isomers of the molecule due to the presence of the bulky Boc protecting groups. These isomers were unevenly populated. Hence, the difference in the intensity of the observed signals in the NMR spectra. The presence of two overlapping peaks eluting at 43.5 and 44.4 min respectively in the LC chromatogram trace at 301 nm with same mass confirmed the presence of two isomers.

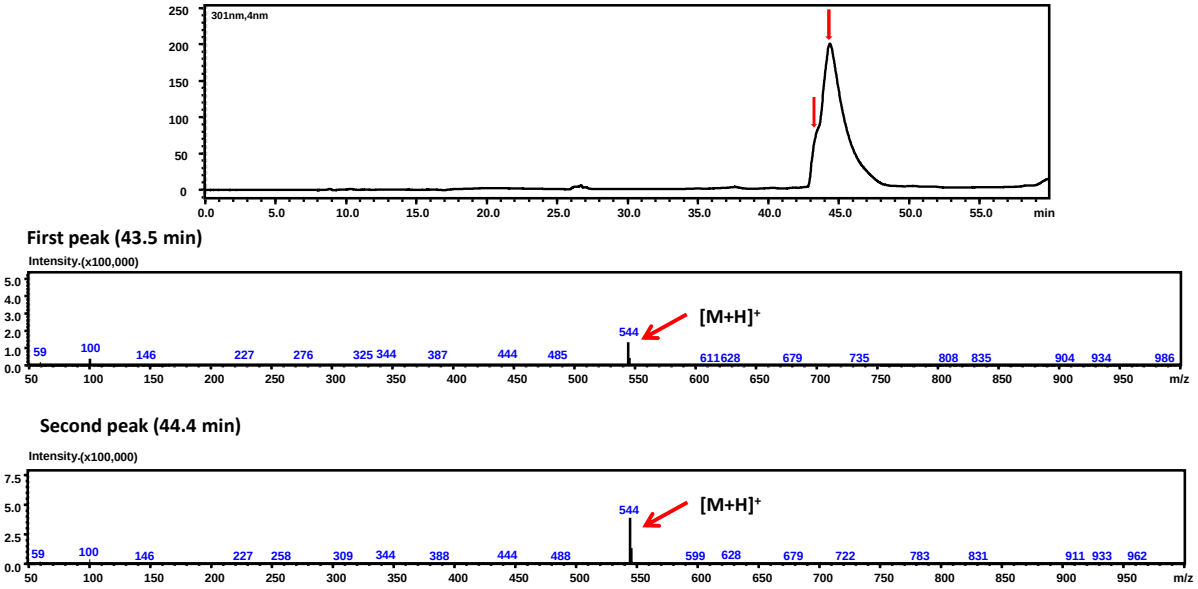

Figure S7. Top: LC trace of compound **7** depicting presence of two peaks in the LC chromatogram trace at 301 nm with same mass but different intensity, indicating the presence of two isomers. Solvent A: 1:1 water: MeOH (0.1 mM NH_4OAc), solvent B: ACN (0.1 mM NH_4OAc), gradient: 5-100% solvent B (0-50 min) 100-5% solvent B (50-60 min); run through Phenomenex Luna C18 (2) column (150 x 4.6 mm). The major elution peaks have been marked with red arrows. Bottom: ESI-MS trace in positive mode corresponding to the peaks eluted at 43.5 and 44.4 min, respectively.

10-(bromomethyl)-5,5-difluoro-1,3,7,9-tetramethyl-5H-dipyrrolo[1,2-c:2',1'-f][1,3,2]diazaborinin-4-ium-5-uide (9): Compound **9** was synthesized according to a previously reported procedure with the following modifications.[4]

2,4-dimethylpyrrole (0.19 mL, 1.8 mmol) was first dissolved in dry DCM (30 mL). The dissolved reagent was added to a solution of bromoacetyl bromide (0.08 mL, 0.9 mmol) in dry DCM (30 mL) under argon. The mixture was then allowed to stir at room temperature for 3 h, in dark. Formation of the intermediate **8** was confirmed by LRMS (ESI). Following this step, triethylamine (2 mL, 0.014 mmol) was slowly added into the reaction mixture over a period of 10 min. Finally, boron trifluoride diethyletherate ($BF_3.OEt_2$) complex (4 mL, 0.03 mmol) was added slowly into the reaction mixture over a period of 15 min. The reaction mixture was allowed to stir at room temperature for 3 h. The reaction was then quenched by adding excess water and the compound was extracted in to DCM

layer. The organic phase was dried over anhydrous sodium sulphate and concentrated under vacuum. The product was purified through column chromatography (silica gel, 30% DCM in hexane) to give compound **9** as a pink crystalline solid (0.045 g, 12%).

^{1}H NMR (600 MHz, $CDCl_3$, 298 K): δ (ppm) 6.09 (2H, s), 4.68 (2H, s), 2.55 (6H, s), 2.53 (6H,s).

^{13}C NMR (150 MHz, $CDCl_3$, 298 K): δ (ppm) 156.47, 140.92, 137.30, 131.01, 24.53, 15.89, 14.67.

LRMS (ESI): Calculated mass for $[M+H]^+$ $C_{14}H_{17}BBrF_2N_2$ 342, observed 341 and 343 indicating the presence of bromine.

All characterization data matched with the previously reported molecule.[4]

10-(azidomethyl)-5,5-difluoro-1,3,7,9-tetramethyl-5H-dipyrrolo[1,2-c:2',1'-f][1,3,2]diazaborinin-4-ium-5-uide (10): Compound **10** was synthesized according to the previously reported procedure, with the following modifications.[5]

Compound **9** (0.03 g, 0.078 mmol) was dissolved in dry methanol (15 mL). To the resulting solution, sodium azide (0.072 g, 1.10 mmol) was added under argon and the reaction mixture was heated at 45 ˚C for 2.5 h. The reaction mixture was cooled to room temperature and was added into excess DCM. The organic layer was washed with water to remove the excess salt. The organic phase was dried over sodium sulphate and concentrated under vacuum. The product was taken forward without further purification.

^{1}H NMR (600 MHz, $CDCl_3$, 298 K): δ (ppm) 6.11 (2H, s), 4.62 (2H, s), 2.54 (6H, s), 2.47 (6H, s).

LRMS (ESI): Calculated mass for $[M+H]^+$ $C_{14}H_{17}BF_2N_5$ 304, observed 304, and 326 = $[M+Na]^+$.

All characterization data matched with the previously reported molecule.[5]

10-((4-(4-(4,13-bis(tert-butoxycarbonyl)-7,10-dimethyl-1,4,7,10,13-pentaazacyclopentadecan-1-yl)phenyl)-1H-1,2,3-triazol-1-yl)methyl)-5,5-difluoro-1,3,7,9-tetramethyl-5H-dipyrrolo[1,2-c:2',1'-f][1,3,2]diazaborinin-4-ium-5-uide (11): Copper sulphate pentahydrate (0.004 g, 0.018 mmol) and sodium-(L)-ascorbate (0.010 g, 0.05 mmol) were dissolved in degassed water separately (2 mL each). A solution of sodium-(L)-ascorbate dissolved in water (2 mL) was added into a dry three-neck round-bottom flask charged with argon. A solution of copper sulphate in water (2 mL) was then added to the reaction mixture. The solution turned deep brown and gradually turned into light orange. Compound **7** (0.02, 0.038 mmol) and compound **10** (0.03 g, 0.099 mol) were dissolved in degassed THF (10 mL) and the solution was added into the reaction mixture containing the active catalyst. The reaction mixture was allowed to stir at room temperature in the dark and under argon atmosphere for 36 h.

The reaction mixture was added to excess DCM and was washed with water to remove salts. The organic layer was dried over sodium sulphate and concentrated under reduced pressure. The compound was purified by column chromatography (neutral alumina, 1% MeOH in DCM) to afford compound **11** as a deep-red solid (0.025 g, 80 %).

^{1}H NMR (400 MHz, $CDCl_3$, 298 K): δ (ppm) 7.65 (2H, m, J= 8 Hz), 7.56 (1H, s), 6.99-6.92 (2H, m, J= 8 Hz), 6.14 (2H, s), 5.86 (2H, s), 3.67 (4H, t, J= 12 hz), 3.42 (4H, s, br), 3.39 (4H, s, br), 2.60 (6H, s), 2.53 (4H, s, br), 2.47 (4H, s), 2.26 (12H, s), 1.56 (18 H, s).

^{13}C NMR (200 MHz, $CDCl_3$, 298 K): 157.85, 155.81, 141.84, 141.79, 139.45, 133.45, 132.57, 127.04, 126.96, 126.83, 124.22, 123.67, 123.13, 116.06, 114.22, 80.39, 65.10, 59.45, 56.15, 49.41, 47.26, 46.23, 45.92, 42.85, 42.32, 33.98, 32.08, 29.31, 29.10, 28.78, 28.65, 27.23, 15.88, 14.95.

HRMS (ESI): Calculated mass for $[M+H]^+$ $C_{44}H_{66}BF_2N_{10}O_4$ 847.5330, observed 847.5333.

Similar to the ^{1}H NMR of compound **7**, the number of peaks was more than the expected (approximately a pair of signals at every ppm value). This was due to the presence of the Boc-protected macrocycle in the molecule, as the Boc-protected macrocycle existed as two rotational isomers. We observed two peaks with very close retention times (46.8 and 47.7 min respectively) in the LC trace that corresponded to the same mass in the mass spectra. We noted that the isomers observed for compound **11** were not

present for **M4** (see next) indicating that the presence of the rotational isomers in compound **11** was due to the Boc groups.

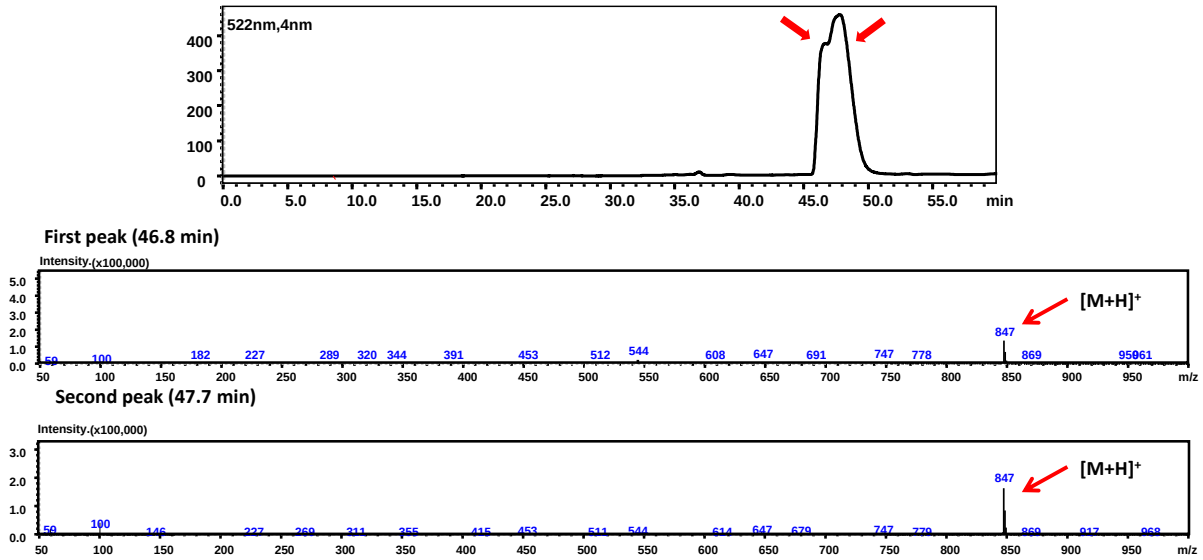

Figure S8. Top: LC trace of compound **11** depicting presence of two peaks in the LC chromatogram trace at 522 nm with same mass but different intensity indicating the presence of two isomers. Solvent A: 1:1 water: MeOH (0.1 mM NH_4OAc), solvent B: ACN (0.1 mM NH_4OAc), gradient: 5-100% solvent B (0-50 min) 100-5% solvent B (50-60 min); run through Phenomenex Luna C18 (2) column (150 x 4.6 mm). The major elution peaks have been marked via a red arrow. Bottom: ESI-MS trace in positive mode corresponding to the peaks eluted at 46.8 and 47.7 min respectively in the LC trace, with peak highlighted with red arrow (lower panel).

10-((4-(4-(7,10-dimethyl-1,4,7,10,13-pentaazacyclopentadecan-1-yl)phenyl)-1H-1,2,3- triazol-1-yl)methyl)-5,5-difluoro-1,3,7,9-tetramethyl-5H-dipyrrolo[1,2-c:2',1'- f][1,3,2]diazaborinin-4-ium-5-uide (M4): Compound **11** (0.004 g, 0.005 mmol) was dissolved in DCM (4 mL) and TFA (1 mL) was added to it. The resulting mixture was then allowed to stir at room temperature for 4 h in dark. The organic layer was concentrated under reduced pressure. **M4** was obtained as a deep orange solid (0.0018 g, 59 %).

^{1}H NMR (600 MHz, CD_3OD, 298 K): δ (ppm) 8.11 (1H, s), 7.73 (2H, d, J= 12 Hz) , 7.01 (2H, d, J= 12 Hz), 6.25 (1H, s), 6.20 (1H, s), 5.98 (2H, s), 3.64 (4H, t, J= 6 Hz), 3.32 (4H, m, br), 3.11 (4H, s, br), 2.61

(10H, m, br), 2.58 (6H, s), 2.53 (6H, s), 2.31 (4H, s).

^{13}C NMR (200 MHz, MeOD, 298 K): 158.57, 158.53, 149.92, 142.93, 134.71, 132.50, 131.75, 128.05, 123.98, 120.17, 114.69, 54.73, 53.20, 47.24, 45.44, 41.48, 32.15, 31.82, 15.74, 14.84.

HRMS (ESI): Calculated mass for $[M+H]^+$ $C_{34}H_{50}BF_2N_{10}$ 647.4281, observed 647.4285.

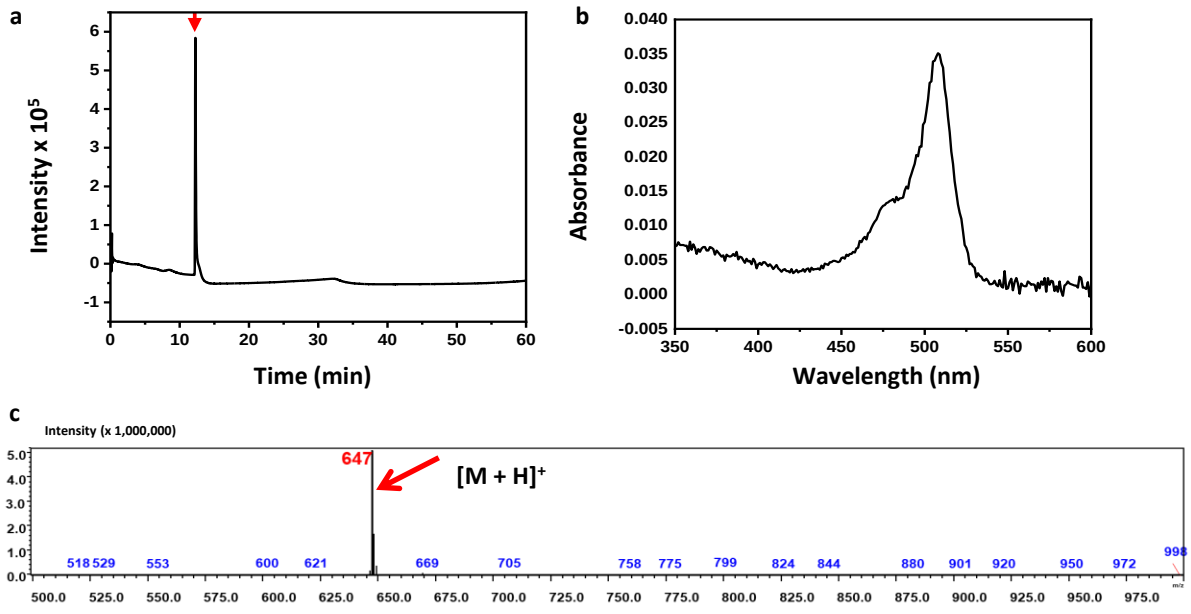

Figure S9. (a) LC trace of **M4** confirming purity (LC depicting absorption intensity at 517 nm). Solvent A: 1:1 water: MeOH (0.1 mM NH_4OAc), solvent B: ACN (0.1 mM NH_4OAc), gradient: 5-100% solvent B (0-50 min) 100-5% solvent B (50-60 min); run through Phenomenex Luna C18 (2) column (150 x 4.6 mm). The major elution peak has been marked via a red arrow. (b) Absorption spectra of **M4** (10 μM) in aqueous buffer containing HEPES (20 mM) and KNO_3 (100 mM) (pH 7.1). (c) ESI-MS trace in positive mode corresponding to the peak eluted in the LC trace, with peak highlighted in red.

Determination of Partition Coefficient (log P) Value of M4

For experimental determination of log P value of **M4**, 5 μM of **M4** was taken in deionized water (400 μL). Absorption of 200 μL of the solution was recorded. The rest 200 μL of the solution was mixed with 1-octanol (200 μL) and the mixture was shaken for 30 min and then the mixture was allowed to stand for 2 h for separation of aqueous and octanol layers. Following that the aqueous layer was carefully

removed and its absorption was recorded. Appropriate solvents were used for baseline measurements. The absorbance value of **M4** at 517 nm, recorded at the beginning of the experiment was considered as absorbance value of aqueous layer at t = 0 h and the absorbance value of the aqueous layer of **M4** at 517 nm, separated from octanol, was considered as absorbance value at t = 2.5 h. These values were used to calculate the log P value of **M4** by using the equation:

$$\log P = \log [(\text{Absorbance at 0 h} - \text{Absorbance at 2.5 h}) / \text{Absorbance at 2.5 h}]$$

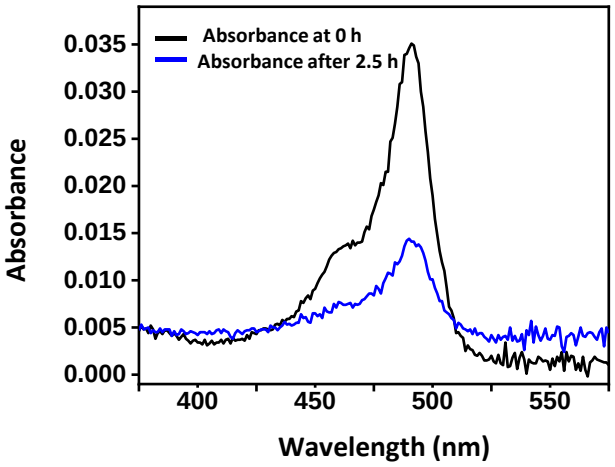

Figure S10. Absorption spectra of **M4** in water at 0 h and after 2.5 h recorded for the calculation of log P.

Determination of Quantum Yield of M4

Quantum yields of **M4** in both absence and presence of Mn^{2+} ions were estimated with respect to fluorescein in 0.1 N NaOH as standard. The concentrations of solutions used for the standard were 0 μM (blank), 0.3 μM, 0.6 μM, 0.9 μM, 1.1 μM, and 1.4 μM. The quantum yield calculations were done based on the reported quantum yield of fluorescein at 480 nm which was 0.95.[6] For the estimation of the quantum yield of **M4** in absence of Mn^{2+} ions, the following solutions were prepared: 0 μM (blank), 0.3 μM, 0.6 μM, 0.9 μM, 1.1 μM, and 1.4 μM solutions of only **M4** in aqueous buffer containing HEPES (20 mM), KNO_3 (100 mM) (pH 7.1). For the estimation of the quantum yield of **M4** in presence of Mn^{2+} ions, the following solutions were prepared: 0 μM (blank), 0.3 μM, 0.6 μM, 0.9 μM, 1.1 μM, and 1.4 μM solutions of only **M4** in aqueous buffer containing $MnCl_2$ (10 μM), HEPES (20 mM), KNO_3 (100 mM) (pH 7.1). Absorption spectra were recorded for all solutions. Fluorescence spectra (λ_{ex}: 480 nm, λ_{em}:

495 to 550 nm for **M4** (both in absence and presence of Mn^{2+}) and λ_{ex}: 480 nm, λ_{em}: 490 to 550 nm for fluorescein) for all solutions were recorded in identical slit width (1 nm x 1 nm). Integrated area for individual fluorescence spectra were plotted against the absorbance (at 480 nm for both **M4** and fluorescein) for each solution. The plot of integrated fluorescence intensity versus absorbance for each fluorophore was fitted to a linear fitting equation. The ratio of the slopes for **M4** to fluorescein was used to calculate the quantum yield of **M4** using the following equation:

$$\phi_{M4} = \phi_{st}(\frac{slope_{M4}}{slope_{st}})(\frac{{\eta_{M4}}^2}{{\eta_{st}}^2})$$

ϕ_{M4} and ϕ_{st} were the quantum yields of **M4** and standard, respectively. $Slope_{M4}$ and $slope_{st}$ were the slopes of the fits obtained from the integrated fluorescence versus absorbance plots of **M4** and the standard, respectively. η_{M4}, η_{st} were the refractive indices of solvents for **M4** and the standard, respectively. For the estimation of quantum yield of **M4**, φ_{st} = 0.95, η_{st}, η_{M4} = 1.33 were used.

Measurements were taken twice for each case and the mean of the quantum yield values for **M4** and **M4** with Mn^{2+} respectively from two independent experiments has been reported.

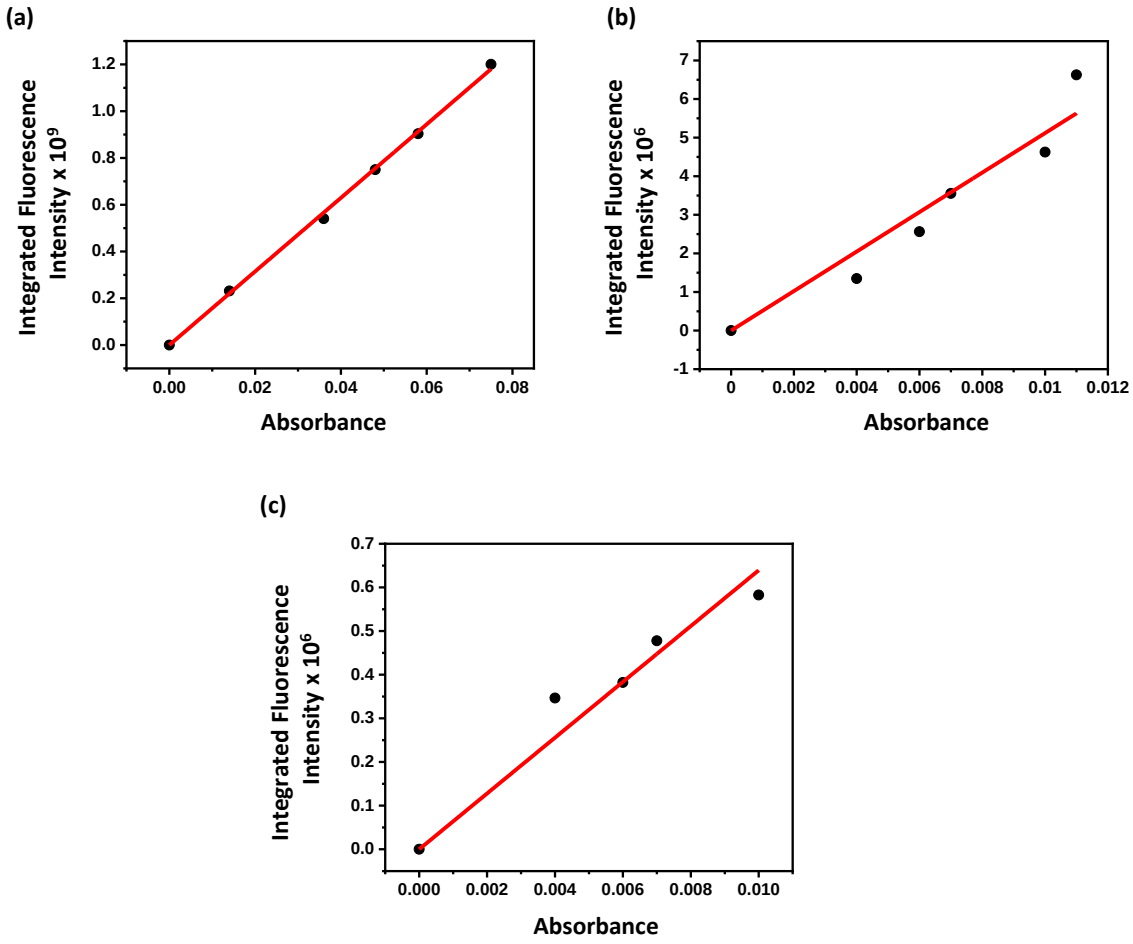

Figure S11. (a) Representative integrated fluorescence vs absorbance plots for fluorescein in 0.1 N NaOH (b) **M4** (c) **M4** in presence of Mn^{2+}. Linear fits (red line) for the data points in the plots yielded slopes 1.58 x 10^{10}, 5.12 x 10^{8}, and 6.39 x 10^{8} for fluorescein, **M4** and **M4** in presence of Mn^{2+}, respectively.

Determination of Extinction Coefficient of M4

Absorption spectra of different concentrations of **M4** were recorded in aqueous buffer (HEPES (20 mM) and KNO_3 (100 mM) pH 7.1). Absorbance values at 508 nm were plotted against concentration. The extinction coefficient was obtained from the slope of the plot from the following equation:

$$\varepsilon = \frac{slope}{l}$$

where ε is the molar extinction coefficient, slope is the slope of the fit obtained from the absorbance versus concentration plots and l is the path length for the beam travel (1 cm). Measurements were taken thrice and the mean of the extinction coefficient values for **M4** has been reported.

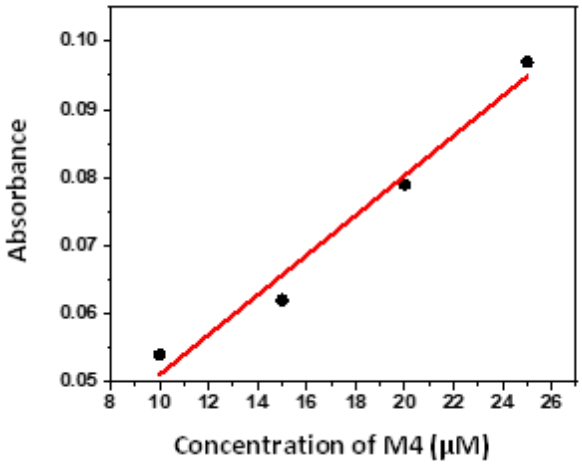

Figure S12. Absorbance vs concentration plot of **M4** in water recorded for the calculation of extinction coefficient.

Determination of Dissociation Constant (K_d) for M4 with Mn^{2+} and Other Metal Ions

Fluorescence spectra were obtained by excitation at 480 nm with slit width 5 nm for both excitation and emission for **M4** with increasing concentration of Mn^{2+} ions. $MnCl_2.4H_2O$ was used as the source of Mn^{2+} unless otherwise stated. The apparent dissociation constants (K_d) were determined from a plot of observed fluorescence intensity (F) over fluorescence intensity of the sensor in the absence of any metal ion (F_0) at 514 nm versus $[Mn^{2+}]$.

The data were fitted to the following equation for **M4**:

$$\frac{F}{F_0} = 1 + (F_{max} - F_0) \times \frac{([L]_t + [Mn^{2+}]_t + K_d) - \sqrt{([L]_t + [Mn^{2+}]_t + K_d)^2 - 4[L]_t[Mn^{2+}]_t}}{2 \times [L]_t \times F_0}$$

..... (1)

where, F_{max} is the fluorescence for the Mn^{2+} bound sensor complex. $[L]_t$ is the total sensor concentration and $[Mn^{2+}]_t$ is the total Mn^{2+} concentration. The same equation was used to fit the fluorescence response curves for Zn^{2+} and Ni^{2+} (Figure S17).

To further validate the K_d values for Ni^{2+} and Zn^{2+}, we performed fluorescence competition titrations by titrating in Ni^{2+}/Zn^{2+} into a solution of the Mn^{2+}-**M4** complex.

We measured the fluorescence of the Mn^{2+}-**M4** complex at the saturation point of the titration data for the probe with Mn^{2+}. Then we titrated in Ni^{2+} to the solution (Figure S18a). The concentration of the **M4** sensor used for the competition titration was 2 μM and Mn^{2+} used was 10 μM (saturation point for Mn binding). Since the K_d ratio of Ni^{2+} to Mn^{2+} was ~ 2, it was expected that 50 % of the sensor would be bound to Ni^{2+} and rest 50 % to Mn^{2+} at a concentration of ~ 20 μM Ni^{2+}. On the basis of binding constants and fluorescence intensities for the Mn^{2+}-**M4** and Ni^{2+}-**M4** complexes, at the ~ 20 μM Ni^{2+} point in the competition titration, we expected a ~1.2 times decrease in the intensity value with respect to the fluorescence intensity value for the Mn^{2+}-**M4** complex. We obtained a 1.3 times intensity decrease at 20 μM Ni^{2+} from the competition titration experiment which distinctly validated the K_d value of the sensor for Ni^{2+}.

The same experiment was performed for Zn^{2+}. We measured the fluorescence of Mn^{2+}-**M4** complex at the saturation point of the titration data for the probe with Mn^{2+}. Then we titrated in Zn^{2+} to the solution (Figure S18b). The concentration of the **M4** sensor used for the competition titration was 2 μM and Mn^{2+} used was 10 μM (saturation point for Mn binding). Since the K_d ratio of Zn^{2+} to Mn^{2+} was ~ 6, it was expected that 50 % of the sensor would be bound to Zn^{2+} and rest 50 % to Mn^{2+} at a concentration of ~ 60 μM Zn^{2+}. On the basis of binding constants and fluorescence intensities for the Mn^{2+}-**M4** and Zn^{2+}-**M4** complexes, at the ~ 60 μM Zn^{2+} point in the competition titration, we expected a ~1.2 times decrease in the intensity value with respect to the fluorescence intensity value for the Mn^{2+}-**M4** complex. We obtained a 1.2 times intensity decrease at 60 μM Zn^{2+} from the competition titration experiment which distinctly validated the K_d value of the sensor for Zn^{2+}.

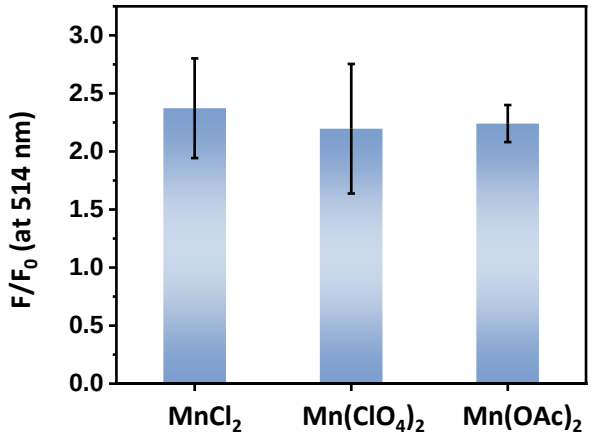

Figure S13. Bar plots representing observed fluorescence intensity (F) of **M4** (2 μM) in aqueous buffer containing HEPES (20 mM) and KNO_3 (100 mM) (pH 7.1) at 514 nm in presence of different salts of Mn^{2+} over initial fluorescence intensity in absence of Mn^{2+} (F_0) of **M4**; [Mn^{2+}] = 15 μM; λ_{ex} = 480 nm. Data are presented as SEM where *n*=3 in each set.

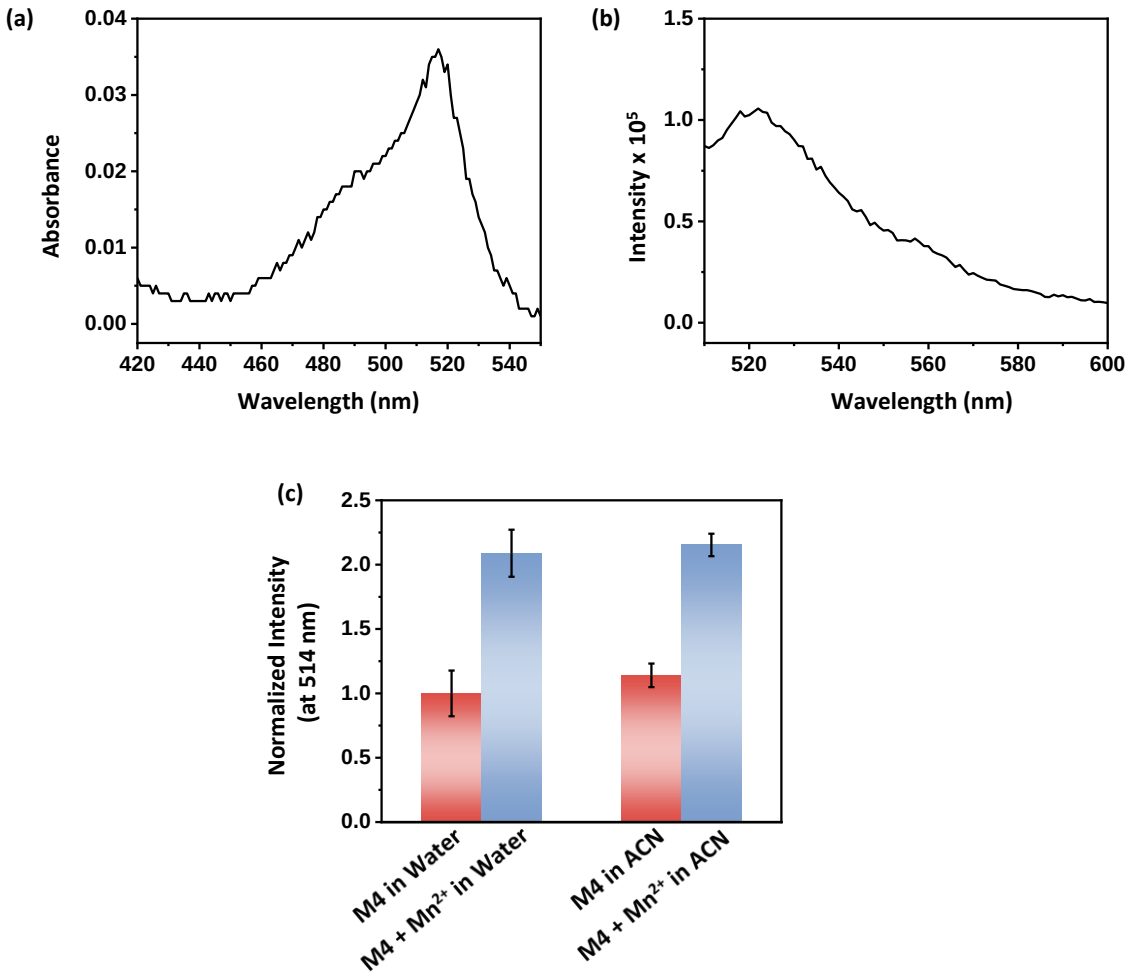

Figure S14. (a) Absorption spectra of **M4** (10 μM) in acetonitrile. (b) Fluorescence emission spectra of **M4** (2 μM) in ACN. (c) Bar plots representing relative increase in fluorescence intensity of **M4** (2 μM) in Mn^{2+} (5 μM) in water and ACN at maxima; λ_{ex} = 480 nm. Intensities are normalized with respect to the intensity of **M4** in water. Data are presented as SEM where *n*=3 in each set.

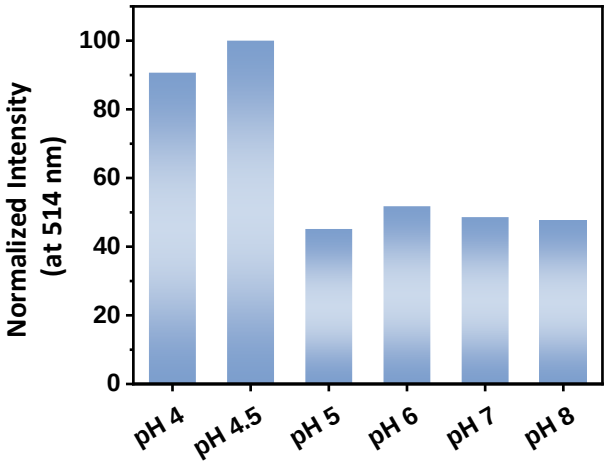

Figure S15. Bar plots representing normalized intensities at 514 nm of **M4** (2 μM) in aqueous buffer containing HEPES (20 mM), KNO_3 (100 mM) (pH 4, 4.5, 5, 6, 7, 8 respectively); λ_{ex} = 480 nm. Intensities were normalized with respect to the intensity of **M4** at pH 4.5.

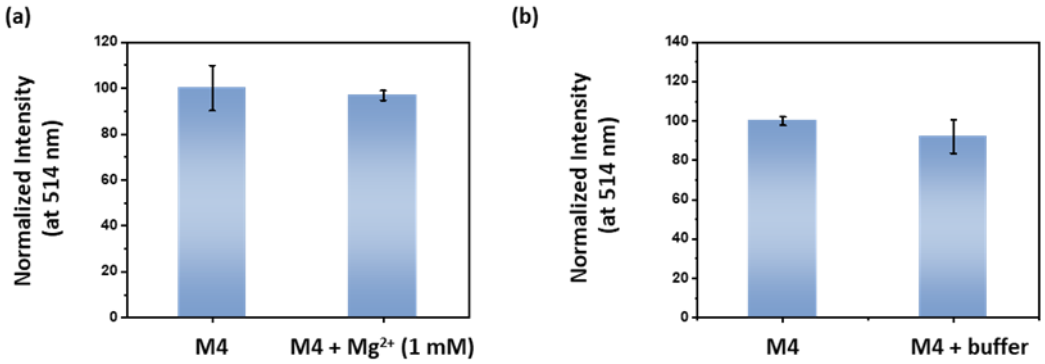

Figure S16. (a) Bar plots representing normalized fluorescence intensity of only **M4** (2 μM) and **M4** (2 μM) in presence of Mg^{2+} (1 mM) in aqueous buffer containing Na-HEPES (20 mM) and KNO_3 (100 mM) (pH 7.1) at 514 nm and; λ_{ex} = 480 nm. Intensities are normalized with respect to the intensity of only **M4**. Data are presented as SEM where *n*=2 in each set. (b) Bar plots representing normalized fluorescence intensity of only **M4** (2 μM) in water and in aqueous buffer containing Na-HEPES (20 mM) and KNO_3 (100 mM) (pH 7.1) at 514 nm and; λ_{ex} = 480 nm. Intensities are normalized with respect to the intensity of **M4** in water. Data are presented as SEM where *n*=3 in each set.

Table S5. Dissociation constant values of **M4** for different biologically relevant metal ions.

METAL ION	Mn (II)	Mg (II)	Ca (II)	Fe (II)	Co (II)	Ni (II)	Cu (II)	Zn (II)
K_D (μM)	1.4 ± 0.2	NR	NR	NR	NR	2.8 ± 0.9	NR	8.0 ± 2.4

* NR = no fluorescence response

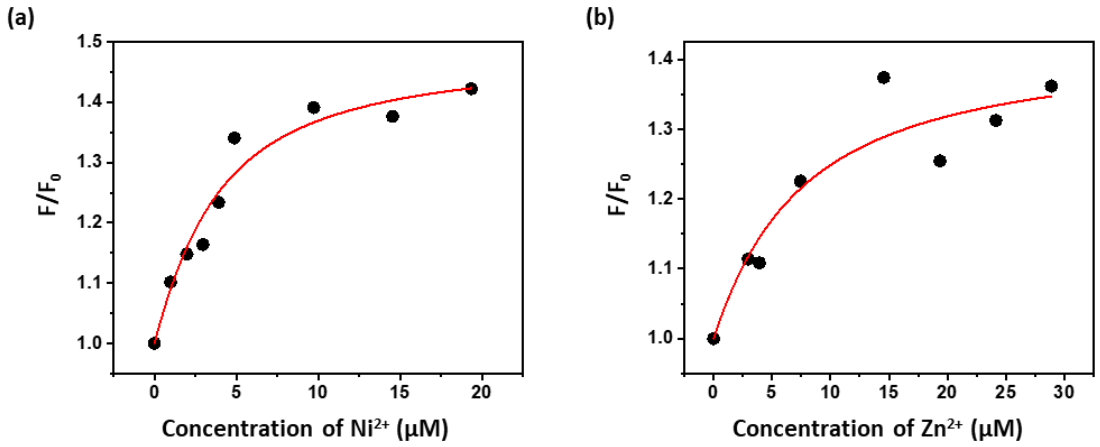

Figure S17. Representative plots depicting observed fluorescence intensity (F) over initial fluorescence intensity of **M4** in absence of M^{2+} (F_0) at 514 nm (black circles; red line is the fitted curve) for (a) Ni^{2+} (b) Zn^{2+}. Each experiment was repeated thrice and the average value of K_d obtained for Ni^{2+} was 2.8 ± 0.9 μM and that for Zn^{2+} was 8.0 ± 2.4 μM.

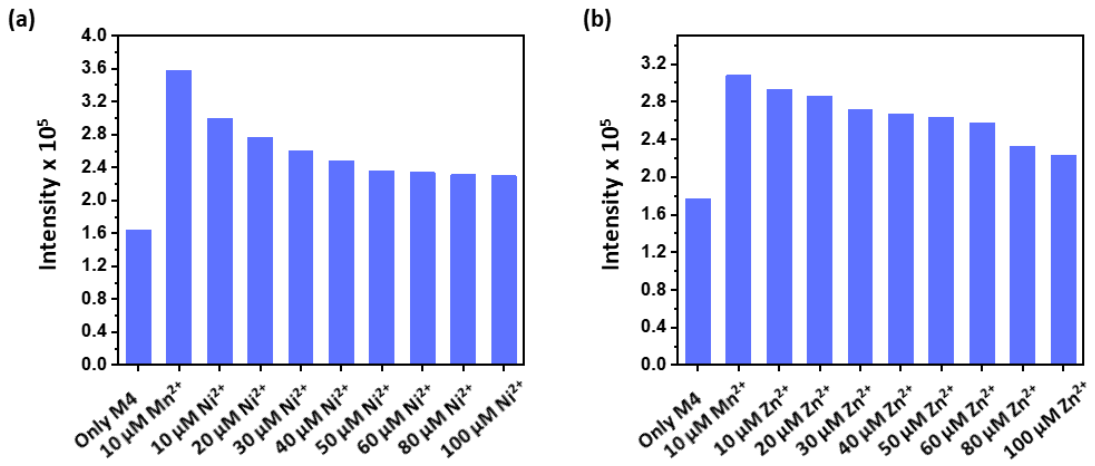

Figure S18. (a) Bar plots representing fluorescence intensity of: only **M4** (2 μM); **M4** (2 μM) in presence of Mn^{2+} (10 μM); and **M4** (2 μM) in presence of Mn^{2+} (10 μM) and Ni^{2+} (10, 20, 30, 40, 50, 60, 80 and

100 μM) in aqueous buffer containing Na-HEPES (20 mM) and KNO_3 (100 mM) (pH 7.1) at 514 nm and; λ_{ex} = 480 nm. (b) Bar plots representing fluorescence intensity of: only **M4** (2 μM); **M4** (2 μM) in presence of Mn^{2+} (10 μM); and **M4** (2 μM) in presence of Mn^{2+} (10 μM) and Zn^{2+} (10, 20, 30, 40, 50, 60, 80 and 100 μM) in aqueous buffer containing Na-HEPES (20 mM) and KNO_3 (100 mM) (pH 7.1) at 514 nm and; λ_{ex} = 480 nm.

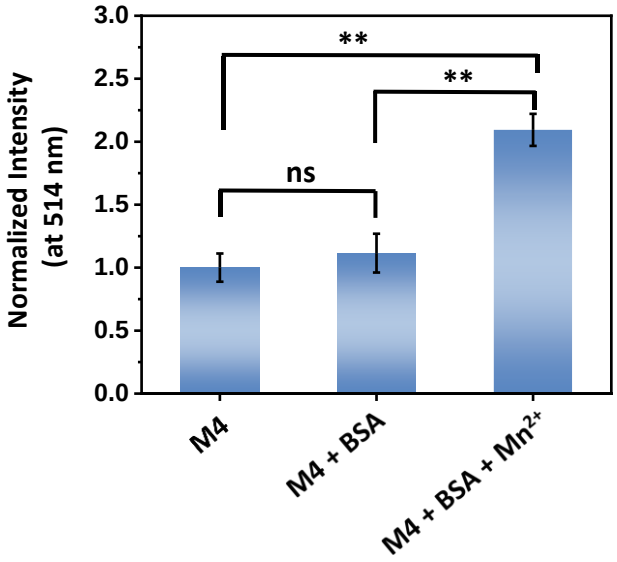

Figure S19. Bar plots representing normalized fluorescence intensity of **M4** (2 μM) in presence of BSA (2 mg/mL) and Mn^{2+} (5 μM) in aqueous buffer containing HEPES (20 mM) and KNO_3 (100 mM) (pH 7.1) at 514 nm; λ_{ex} = 480 nm. Intensities are normalized with respect to the intensity of **M4** in water. Data are presented as SEM where *n*=3 in each set. **p* < 0.05, ***p* < 0.01 and ****p* < 0.001.

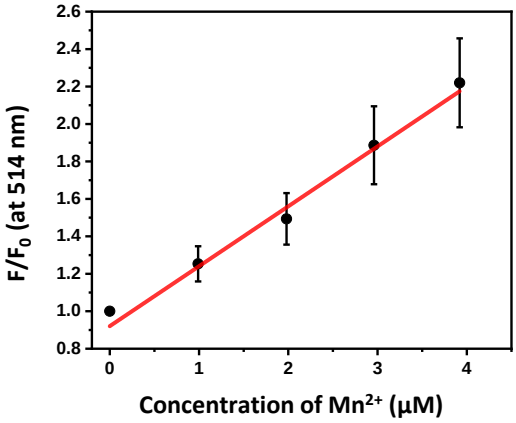

Figure S20. Fluorescence response of **M4** (2 μM) with increasing concentrations of Mn^{2+} ions in aqueous buffer containing HEPES (20 mM) and KNO_3 (100 mM); λ_{ex} = 480 nm. The limit of detection was calculated by using the formula 3σ/k where σ was the standard deviation and k was the slope obtained from the F/F_0 at 514 nm versus Mn^{2+} concentration plot. The LOD calculated was 0.62 ± 0.07 μM.

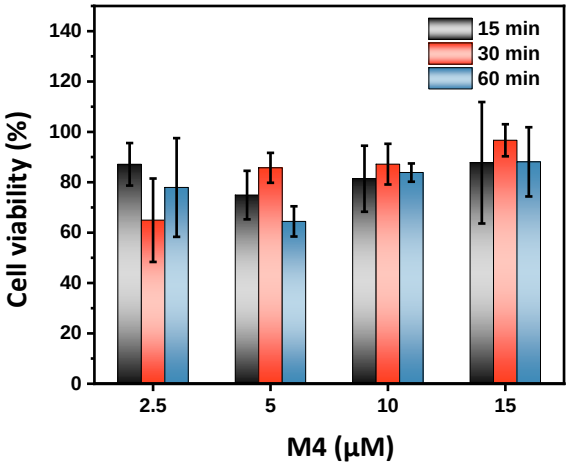

Figure S21. Cell viability in the presence of **M4** at different concentrations (0, 2.5, 5, 10 and 15 μM) in HEK293T cells after 15 min, 30 min, and 1 h of incubation at 37 °C in DMEM, pH 7.4. Percentage of viable cells was determined using MTT assay. Error bars represent the standard deviation of three replicate experiments.

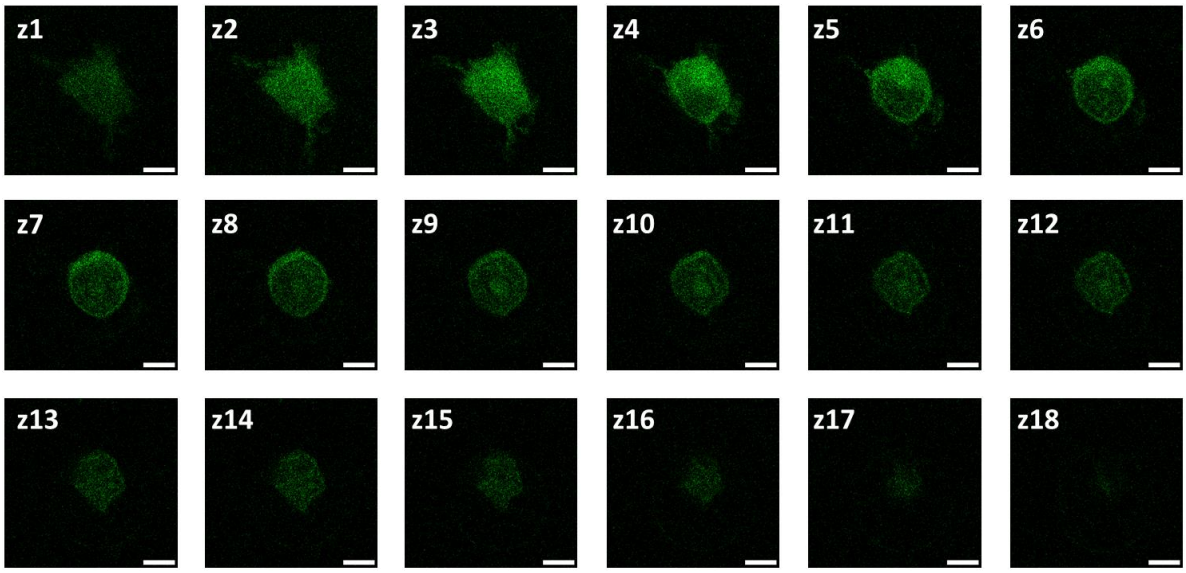

Figure S22. Representative confocal single z plane images of same HEK293T cell (z1 to z18; 1 µm apart) depicting cell permeability of **M4**. Cells were incubated with 5 µM of **M4** in aqueous buffer for 15 min, then washed with aqueous buffer and imaged; λ_{ex} = 488 nm; λ_{em}: 500-600 nm.

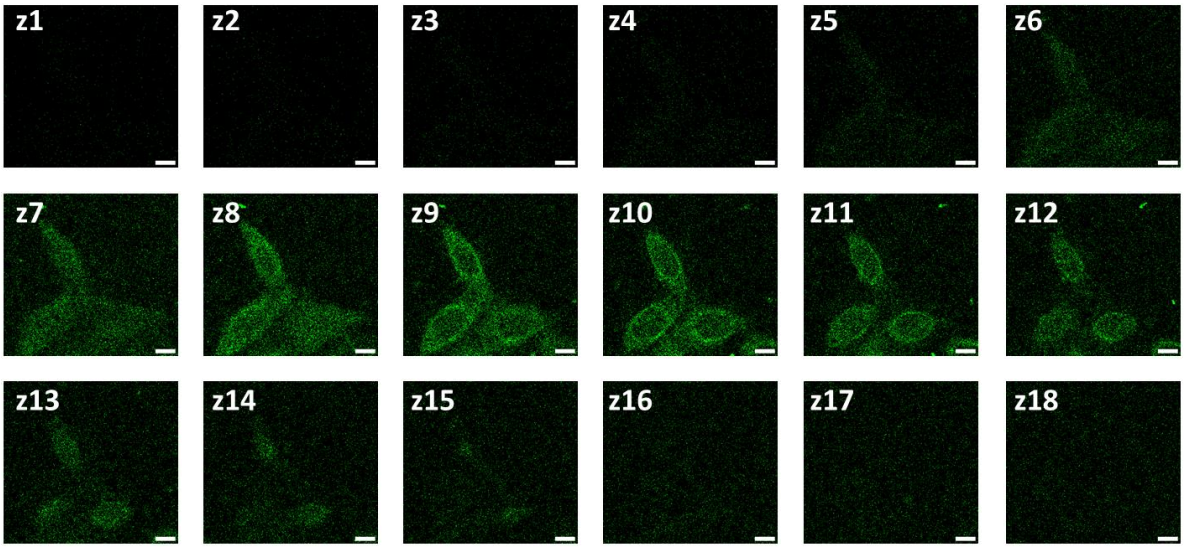

Figure S23. Representative confocal single z plane images of same HeLa cells (z1 to z18; 1 µm apart) depicting cell permeability of **M4**. Cells were incubated with 5 µM of **M4** in aqueous buffer for 15 min, then washed with aqueous buffer and imaged; λ_{ex} = 488 nm; λ_{em}: 500-600 nm.

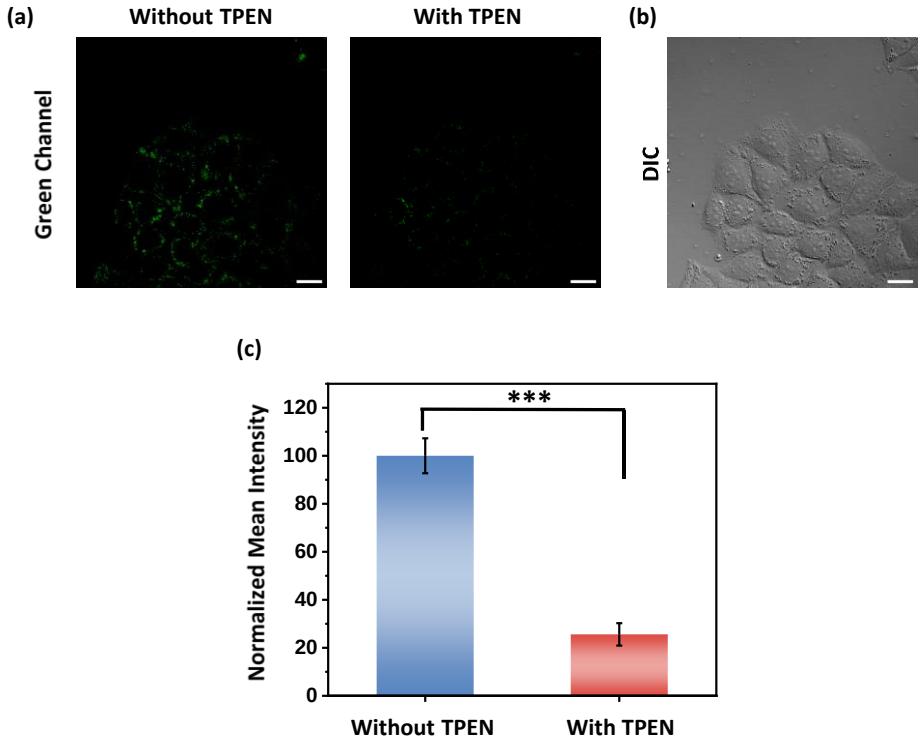

Figure S24. (a) Representative confocal single z plane images of HeLa cells before addition of TPEN and 40 min after addition of TPEN. Cells were incubated with **M4** (5 μM) in aqueous buffer (pH 7.4) for 15 min, washed following which the first image was recorded (Left). Then TPEN (50 μM) was added and the image on right was recorded after 40 min of TPEN addition. λ_{ex} = 488 nm. Scale bar = 20 μm. (b) Differential interference contrast image. (c) Bar plots representing the mean intensities obtained from intensity analysis of confocal images of HeLa cells, shown in (a). Intensity data were normalized to intensity of TPEN-untreated cells. Data are presented as SEM, where n = 5 for each set. *p < 0.05, **p < 0.01 and ***p < 0.001. Fluorescence intensity analyses of confocal images were carried out by using ImageJ software.

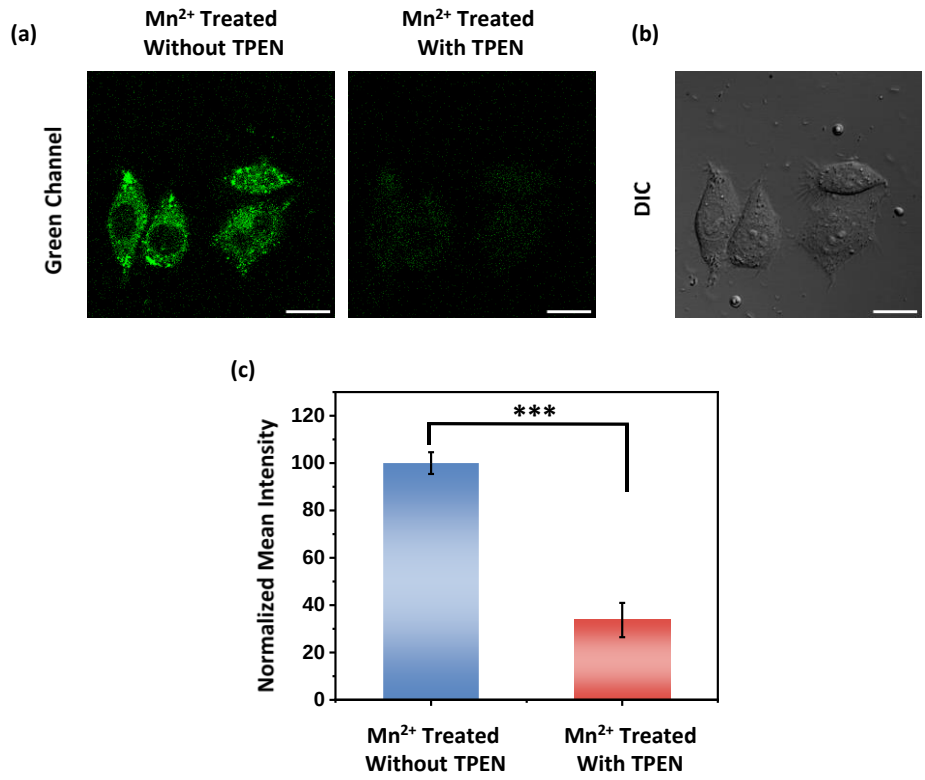

Figure S25. (a) Representative confocal single z plane images of Mn^{2+} treated HeLa cells before addition of TPEN and 40 min after addition of TPEN. Cells were incubated with Mn^{2+} (25 μM) in aqueous buffer (pH 7.4) for 1 h, washed and then incubated with **M4** (5 μM) in aqueous buffer (pH 7.4) for 15 min, washed following which the first image was recorded (Left). Then TPEN (250 μM) was added and the image on right was recorded after 40 min of TPEN addition. λ_{ex} = 488 nm. Scale bar = 20 μm. (b) Differential interference contrast image. (c) Bar plots representing the mean intensities obtained from intensity analysis of confocal images of HeLa cells, shown in (a). Intensity data were normalized to intensity of TPEN-untreated cells. Data are presented as SEM, where n = 5 for each set. *p < 0.05, **p < 0.01 and ***p < 0.001. Fluorescence intensity analyses of confocal images were carried out by using ImageJ software.

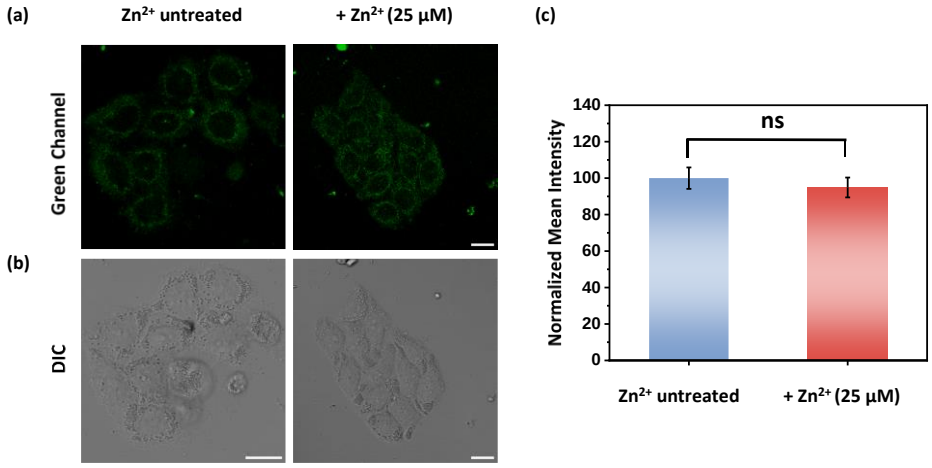

Figure S26. (a) Representative confocal single z plane images of HeLa cells. Cells were incubated with: **M4** (5 µM) in aqueous buffer (pH 7.4) for 15 min (left panel); with 25 µM of Zn^{2+} (added as $Zn(NO_3)_2.6H_2O$) in aqueous buffer (pH 7.4) for 1 h, washed and then incubated with **M4** in aqueous buffer (pH 7.4) for 15 min (right panel). Both the sets were washed with aqueous buffer (pH 7.4) and imaged. λ_{ex} = 488 nm. Scale bar = 20 µM. (b) Differential interference contrast images. Scale bar = 20 µm. (c) Bar plots representing the mean intensities obtained from intensity analysis of confocal images of HeLa cells, shown in (a). Intensity data were normalized to intensity of Zn^{2+} treated cells. Data are presented as SEM, where n = 6 for each set. *p < 0.05, **p < 0.01 and ***p < 0.001. Fluorescence intensity analyses of confocal images were carried out by using ImageJ software.

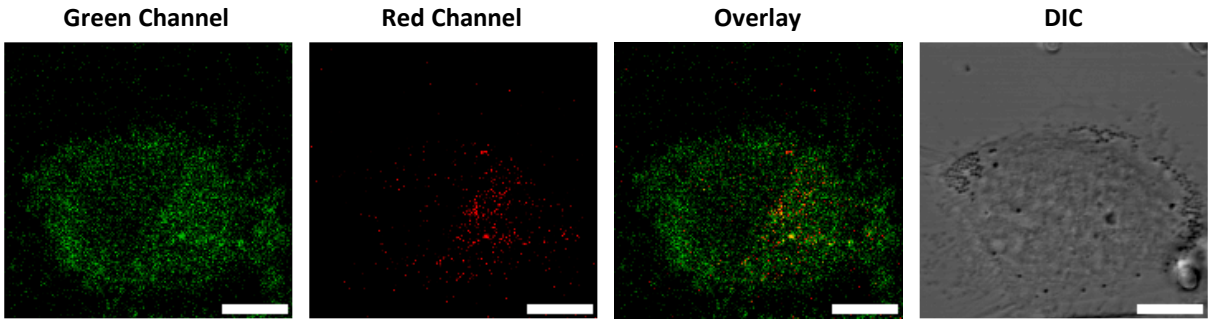

Figure S27. Representative confocal single z plane images of HeLa cell. Cells were incubated with Lysotracker Red (100 nM) for 20 min, washed and incubated with **M4** (5 µM) for 15 min, washed and imaged. Scale bar = 10 µm. λ_{ex} = 488 nm for **M4**, 543 nm for Lysotracker Red.

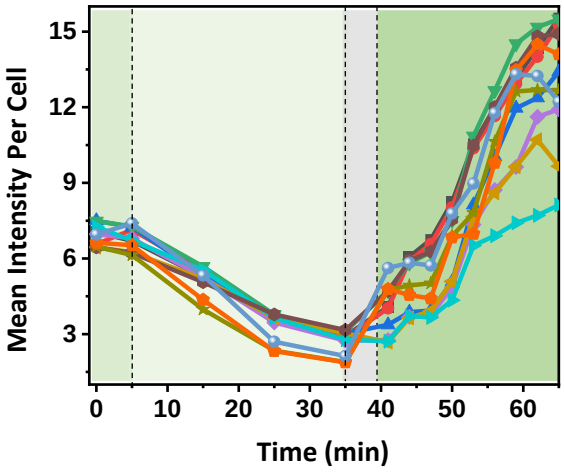

Figure S28. Titration curves corresponding to individual cells representing intracellular Mn^{2+} responses with **M4** for estimation of intracellular labile Mn^{2+} concentrations. Cells were incubated with **M4** (5 μM) in aqueous buffer (pH 7.4) for 15 min, washed and imaged to get the resting state (0-5 min). Next the cells were treated with TPEN (50 μM) and subsequent time-dependent images were taken. After 30 min, cells were washed with aqueous buffer and Mn^{2+} (25 μM) was added and subsequent time-dependent images were taken till saturation was achieved. *n*=4 cells (for each independent experiment, *N*=3).

Table S6. Time resolved fluorescence data for **M4** in absence and presence of Mn^{2+} ions.

Condition	Repeats	τ_1 (ns)	α_1 (%)	τ_2 (ns)	α_2 (%)	τ_3 (ns)	α_3 (%)	Mean Lifetime
M4	1	0.07 ± 0.01	83	0.89 ± 0.16	7	4.56 ± 0.07	10	0.56 ± 0.17
	2	0.07 ± 0.01	84	0.82 ± 0.14	8	3.94 ± 0.08	8	0.42 ± 0.16
	3	0.08 ± 0.01	82	1.04 ± 0.16	9	4.19 ± 0.08	9	0.56 ± 0.18
M4 + Mn^{2+}	1	0.08 ± 0.01	73	1.06 ± 0.21	10	4.69 ± 0.06	17	0.97 ± 0.21
	2	0.07 ± 0.01	75	1.01 ± 0.18	9	4.70 ± 0.05	16	0.90 ± 0.19
	3	0.08 ± 0.01	77	1.07 ± 0.17	9	4.70 ± 0.06	14	0.79 ± 0.18

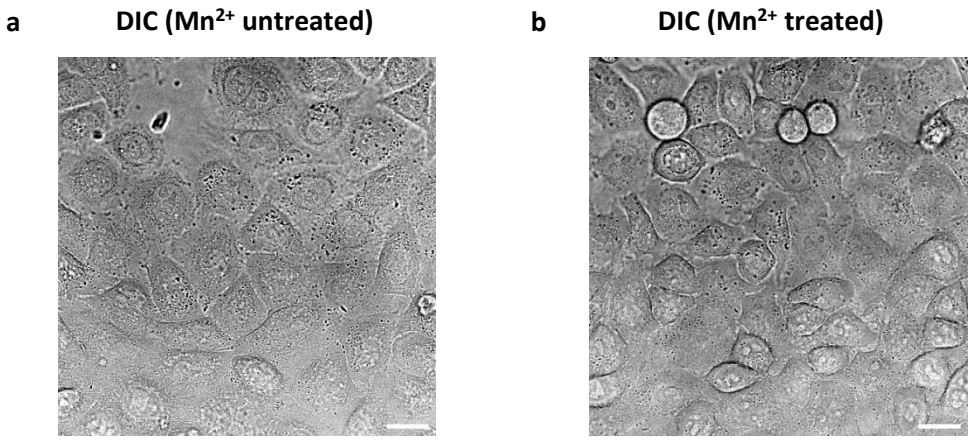

Figure S29. Differential interference contrast images of the cells represented in Figure 4b. Scale bar 20 µm.

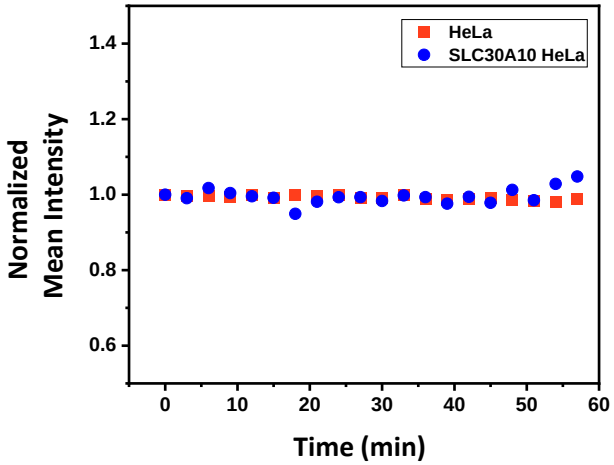

Figure S30. Variation of mean fluorescence intensity of **M4** in HeLa cells (orange squares) and SLC30A10 transfected HeLa cells (blue circles) with time, depicting photo-stability of **M4**. Cells were incubated with 5 µM of **M4** in aqueous buffer (pH 7.4) for 15 min, washed with aqueous buffer and then imaged for 1 h at an interval of 3 min.

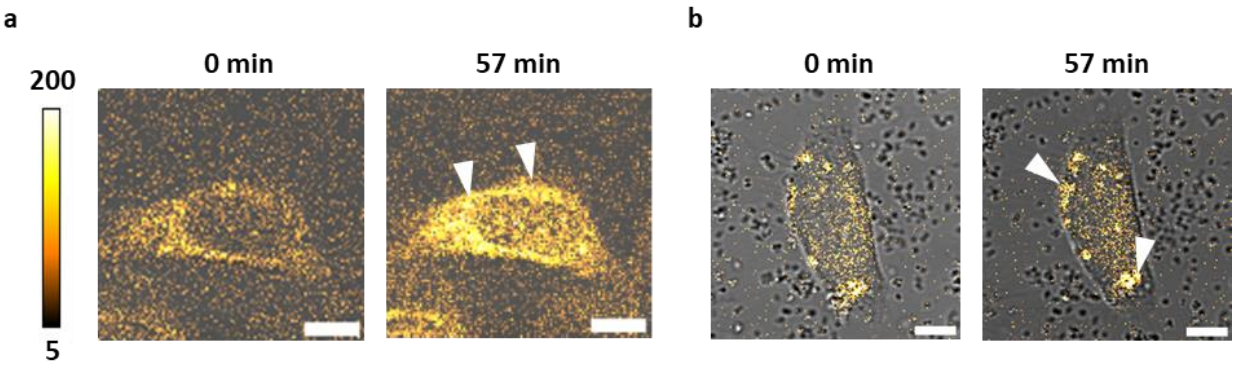

Figure S31. (a) Zoomed-in representative overlay single z plane images of single HeLa cell incubated with **M4** (5 μM) for 15 min before and 1 h after addition of Mn^{2+} (25 μM) respectively. White arrows indicate the regions of maximum increase in fluorescence inside the cell. (b) Zoomed-in representative confocal single z plane images of *SLC30A10* transfected single HeLa cell incubated with **M4** (5 μM) for 15 min before and 1 h after addition of Mn^{2+} (25 μM) respectively. White arrows indicate the regions of maximum increase in fluorescence inside the cell; λ_{ex} = 488 nm; λ_{em}: 500-600 nm. Scale bar 10 μm.

Intensity Analysis of Images

For processing and analysis of confocal microscopy images, Fiji (ImageJ, NIH, USA) software was used. For Figure 3e analysis was done using 5 unique cells from different plates for each condition. The fluorescence intensity analysis was performed using ImageJ software. For intensity analysis, regions of interest (ROIs) were drawn around single cells. The intensity of each selection region was obtained using the 'Measure' tool. Error bars denote standard error of mean (SEM; *n* = 5). For Figure 5e, the entire frame was selected as ROI. The mean intensity of each frame was plotted against time. For Figure S24c and Figure 25c, five unique cells from different plates for each condition were taken for analysis. The intensity analysis was done using the same method as that of Figure 3e. For Figure S26c, analysis was done using six unique cells from different plates for each condition. The intensity analysis was done using the same method as that of Figure 3e. In figure 24a, 26a and 27, the mean fluorescence intensities of all the channels have been multiplied by 2 for better visualization.

Video S1. Fluorescence confocal microscopy video depicting the live uptake dynamics of Mn^{2+} ions in HeLa cells that have inherently low levels of SLC30A10. Scale bar 20 μm.

Video S2. Fluorescence confocal microscopy video depicting the live uptake of Mn^{2+} ions in *SLC30A10* transfected HeLa cells. Scale bar 20 μm.

^{1}H and ^{13}C NMR Spectra

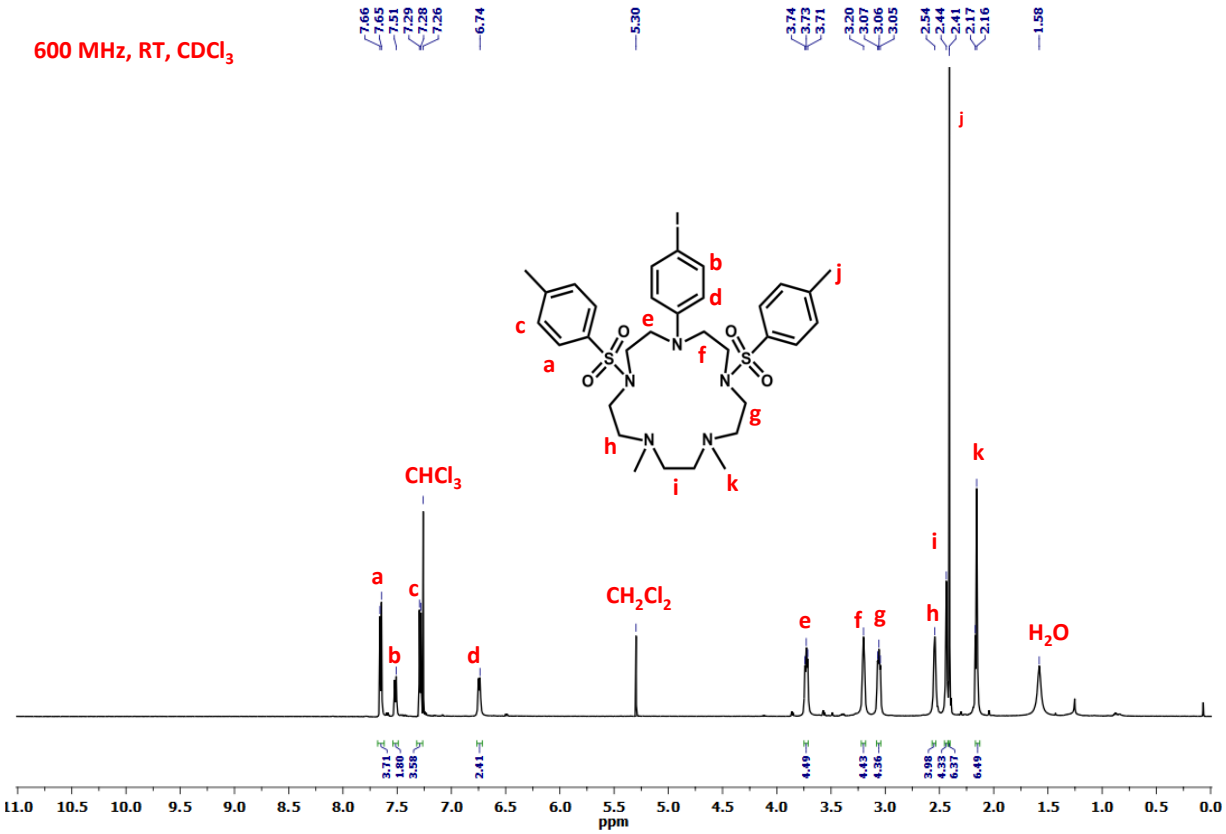

Figure S32. ^{1}H NMR spectrum of compound **4**.

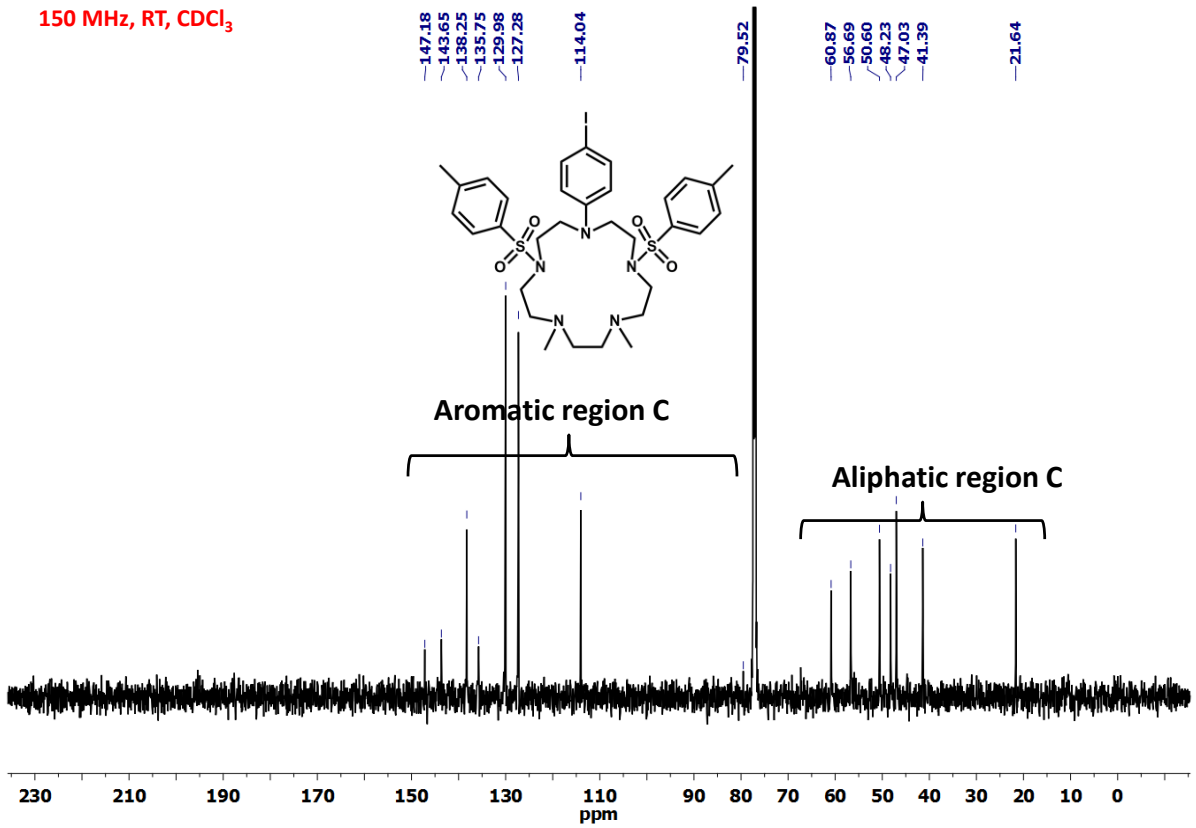

Figure S33. ^{13}C NMR spectrum of compound **4**.

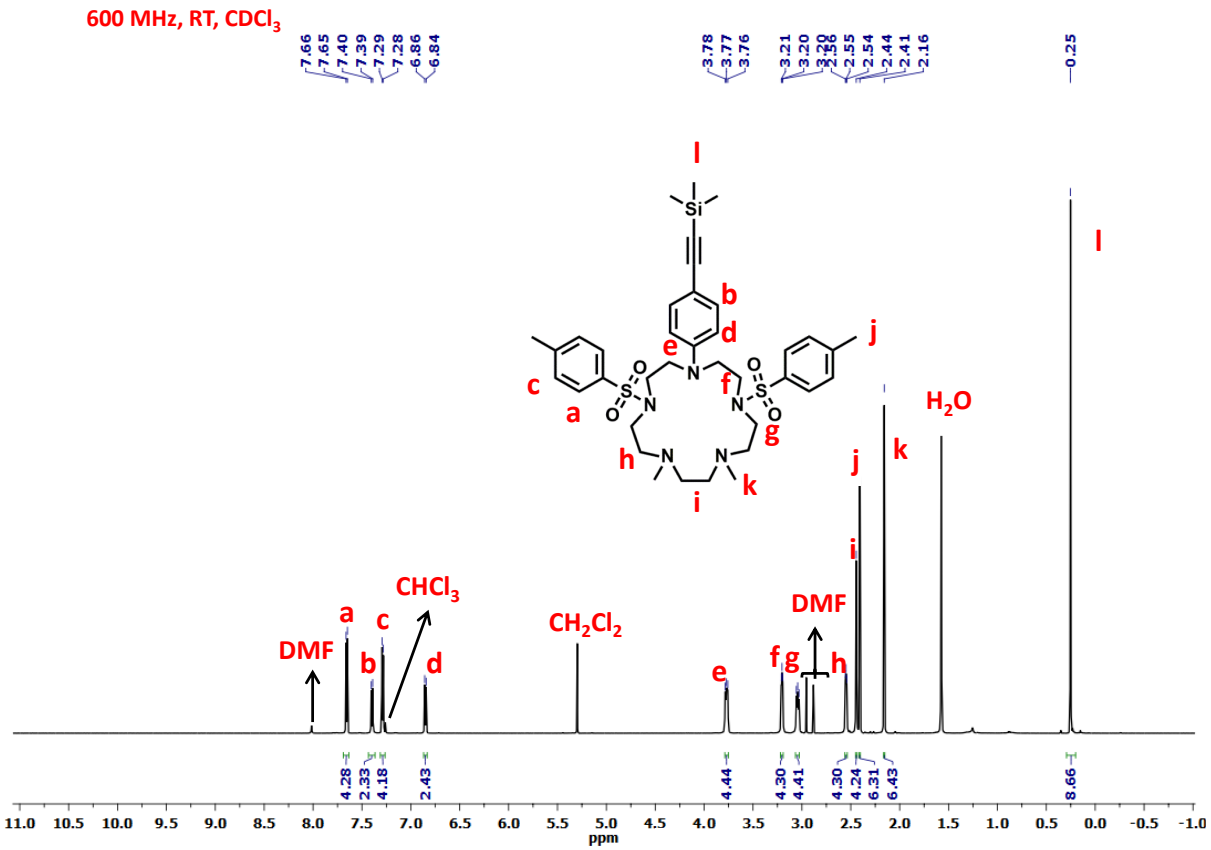

Figure S34. ^{1}H NMR spectrum of compound **5**.

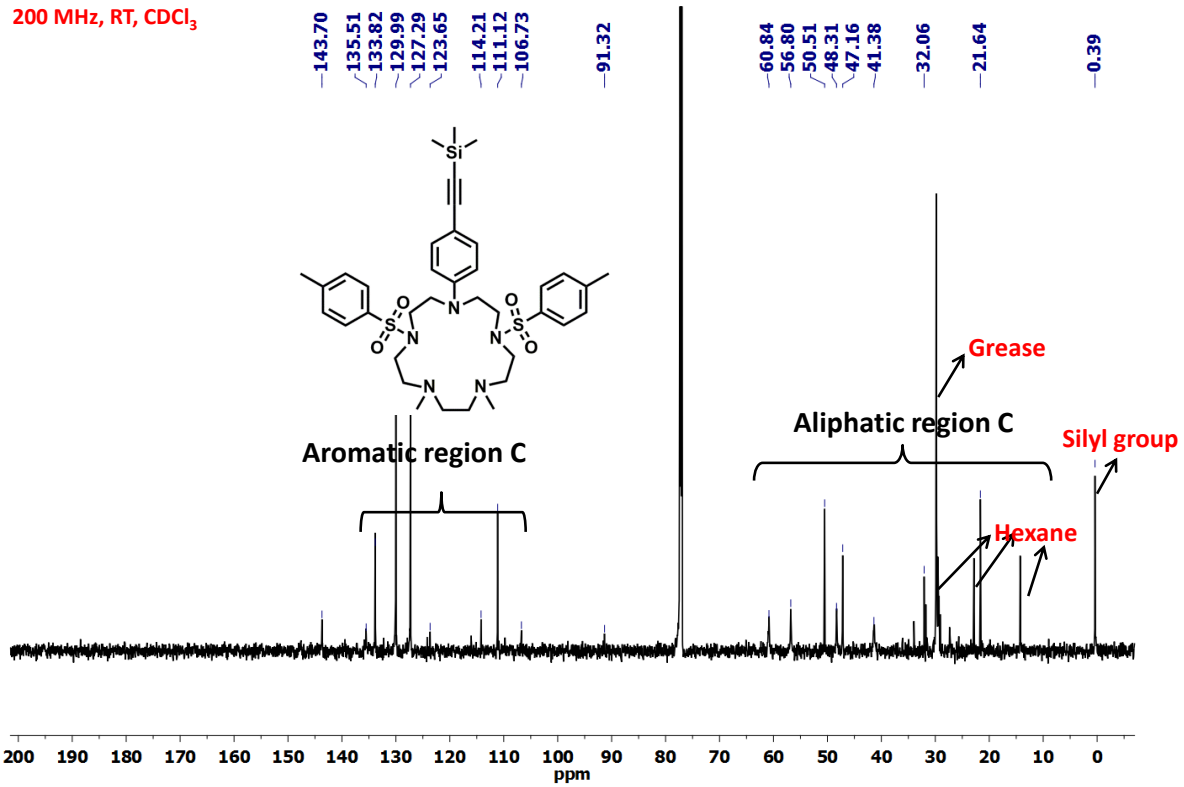

Figure S35. ^{13}C NMR spectrum of compound **5**.

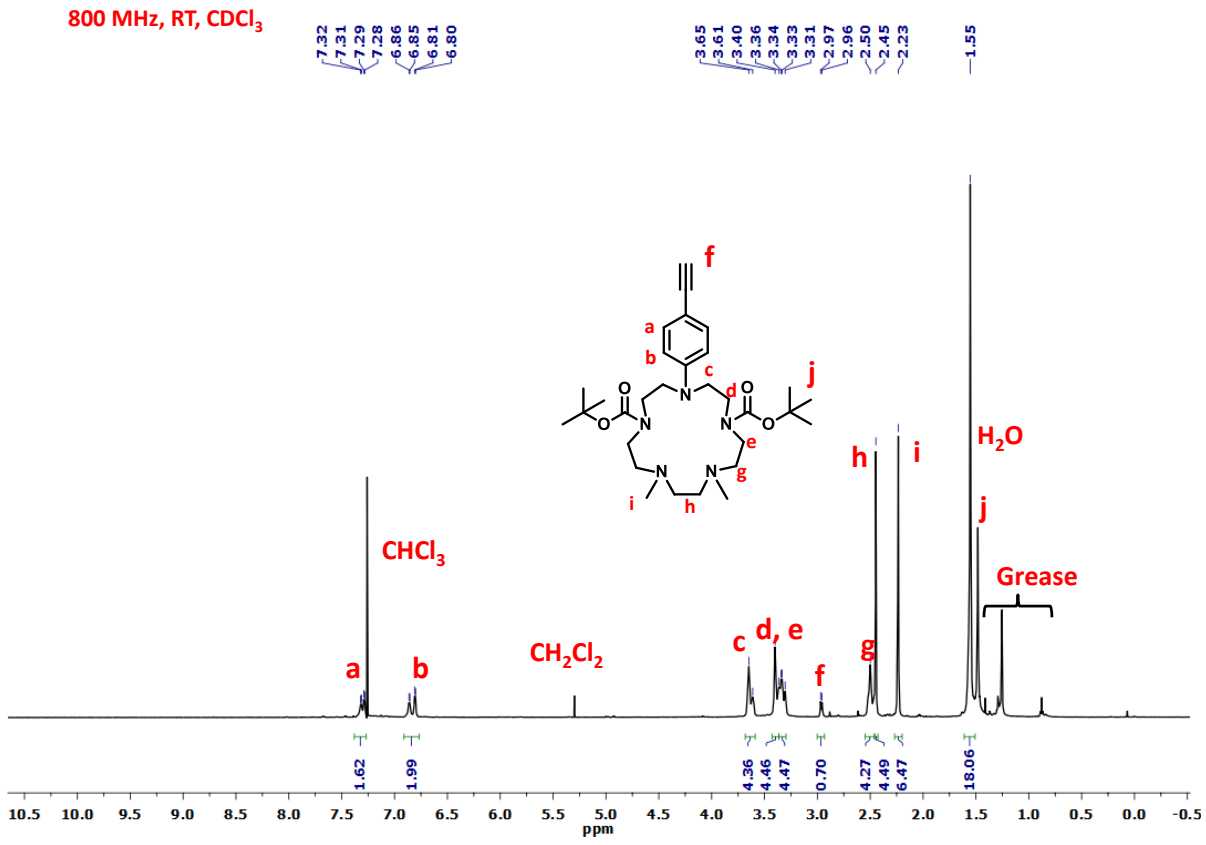

Figure S36. ^{1}H NMR spectrum of compound **7**.

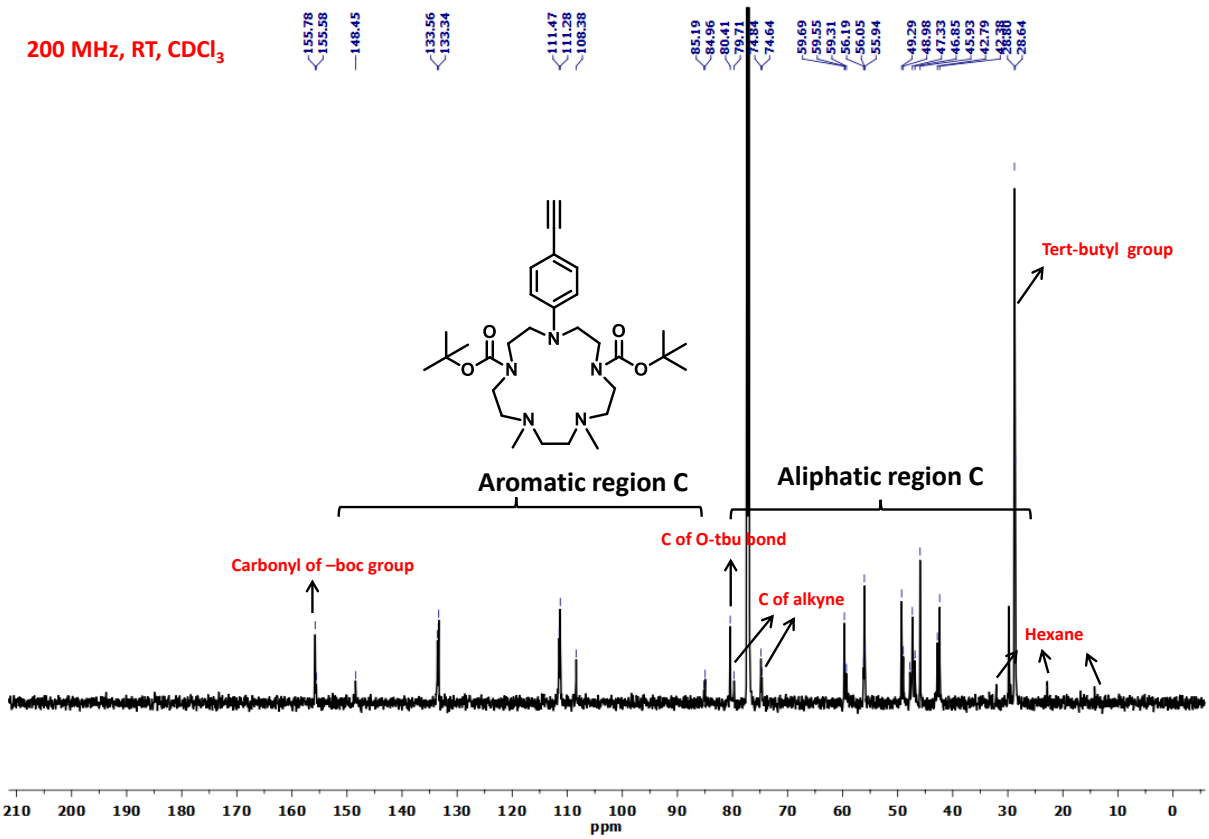

Figure S37. ^{13}C NMR spectrum of compound **7**.

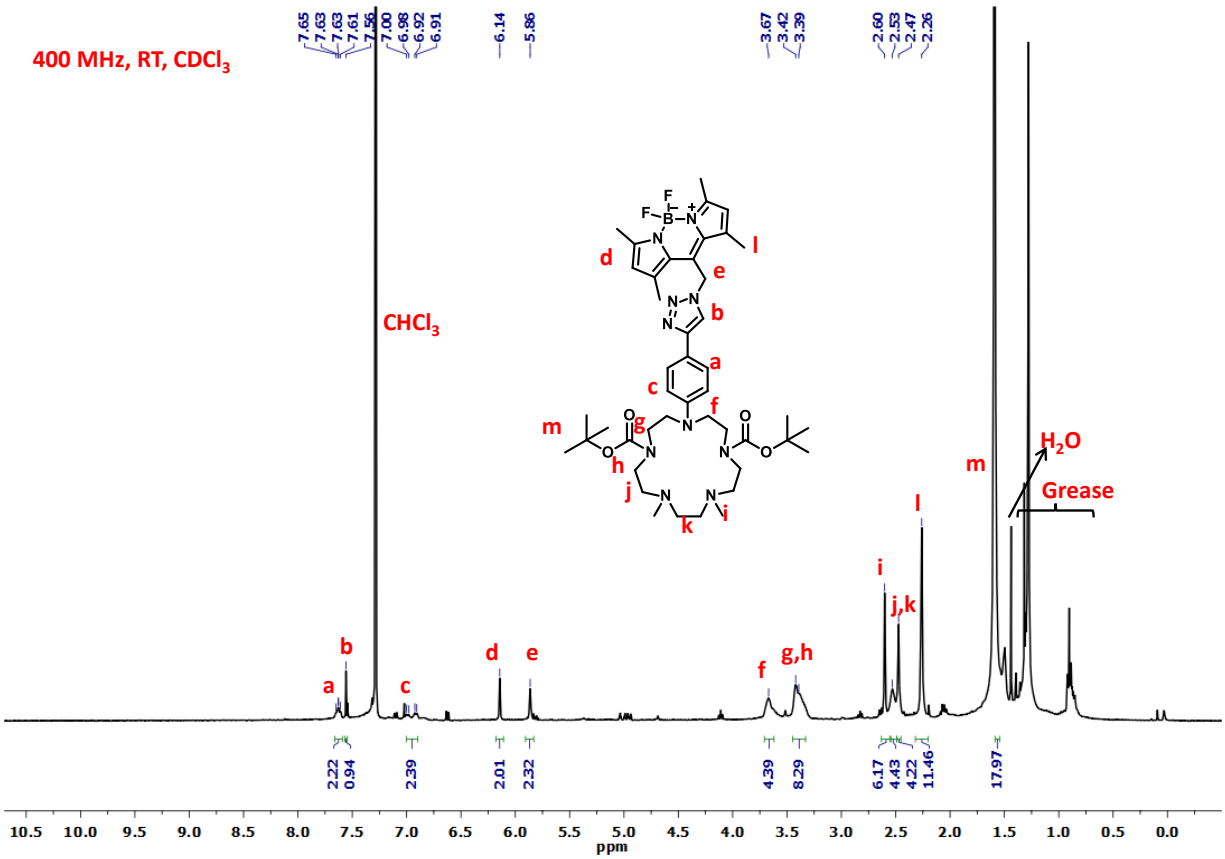

Figure S38. ^{1}H NMR spectrum of compound **11**.

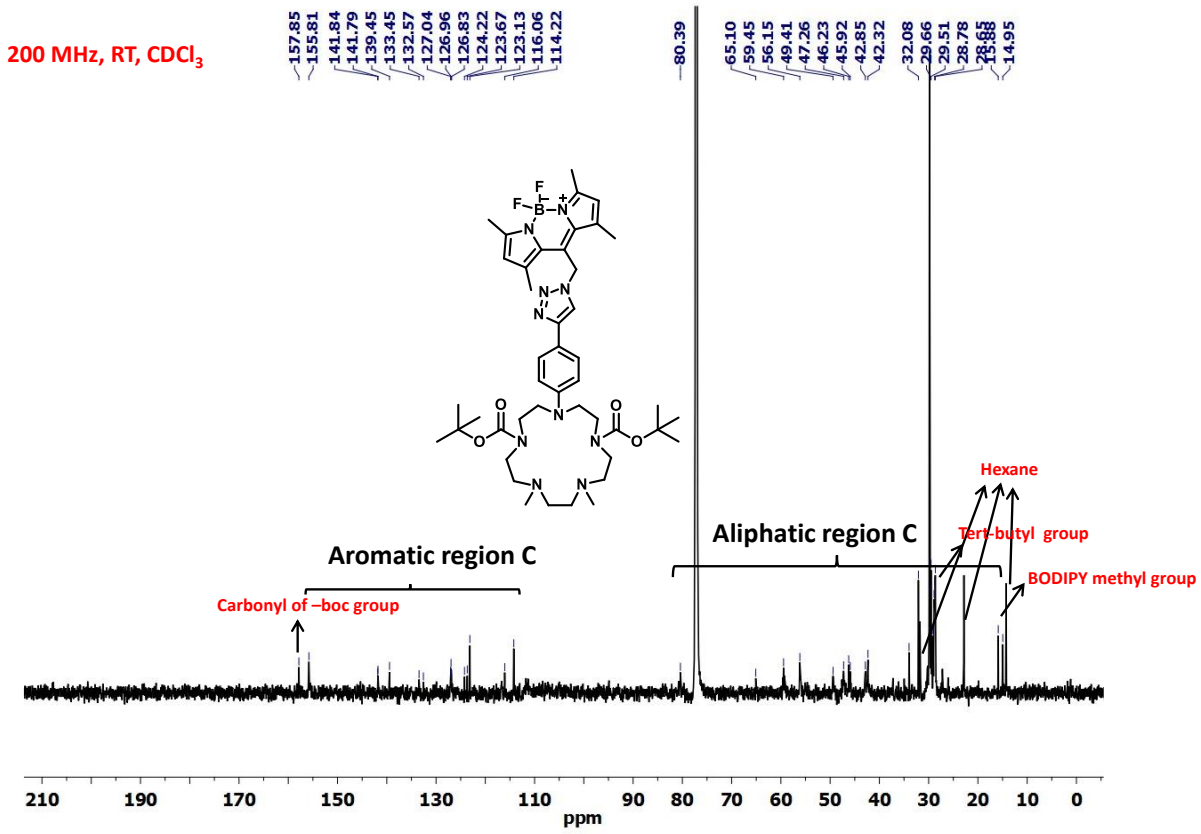

Figure S39. ^{13}C NMR spectrum of compound **11**.

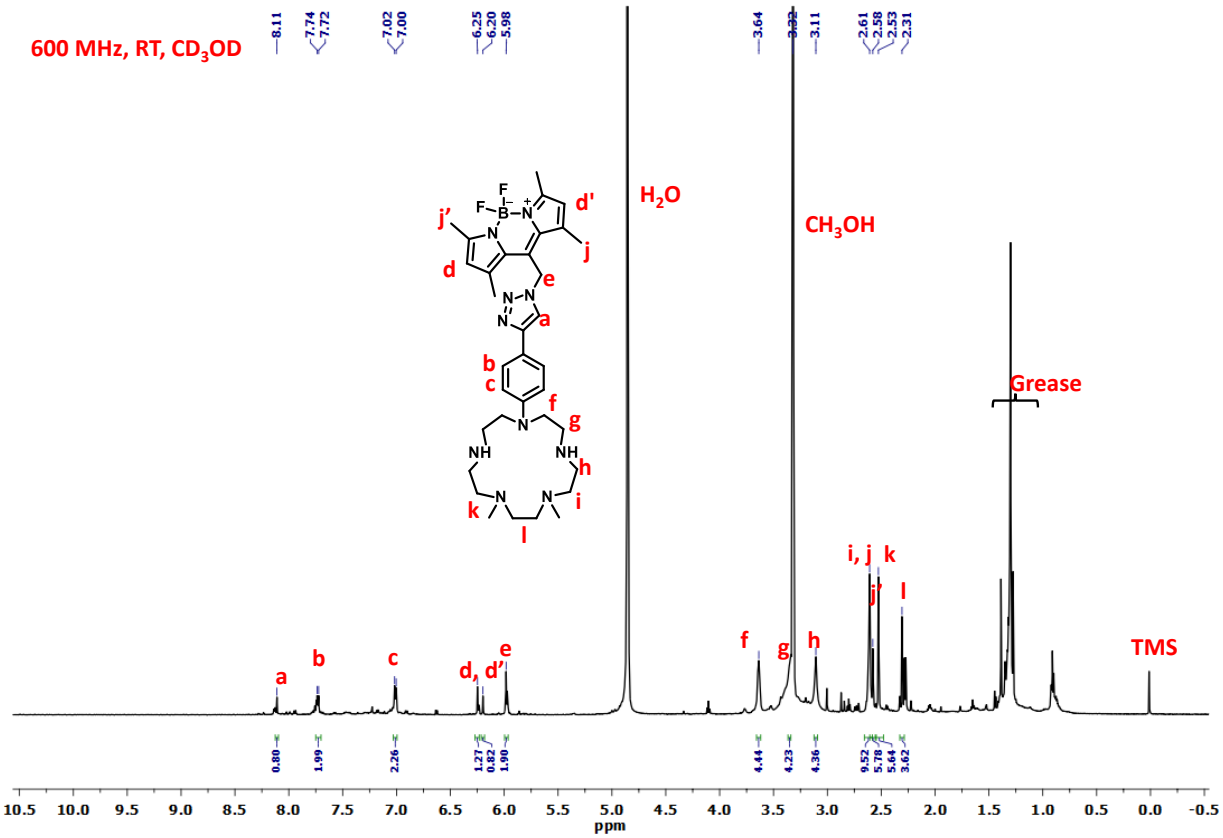

Figure S40. ^{1}H NMR spectrum of compound **M4**.

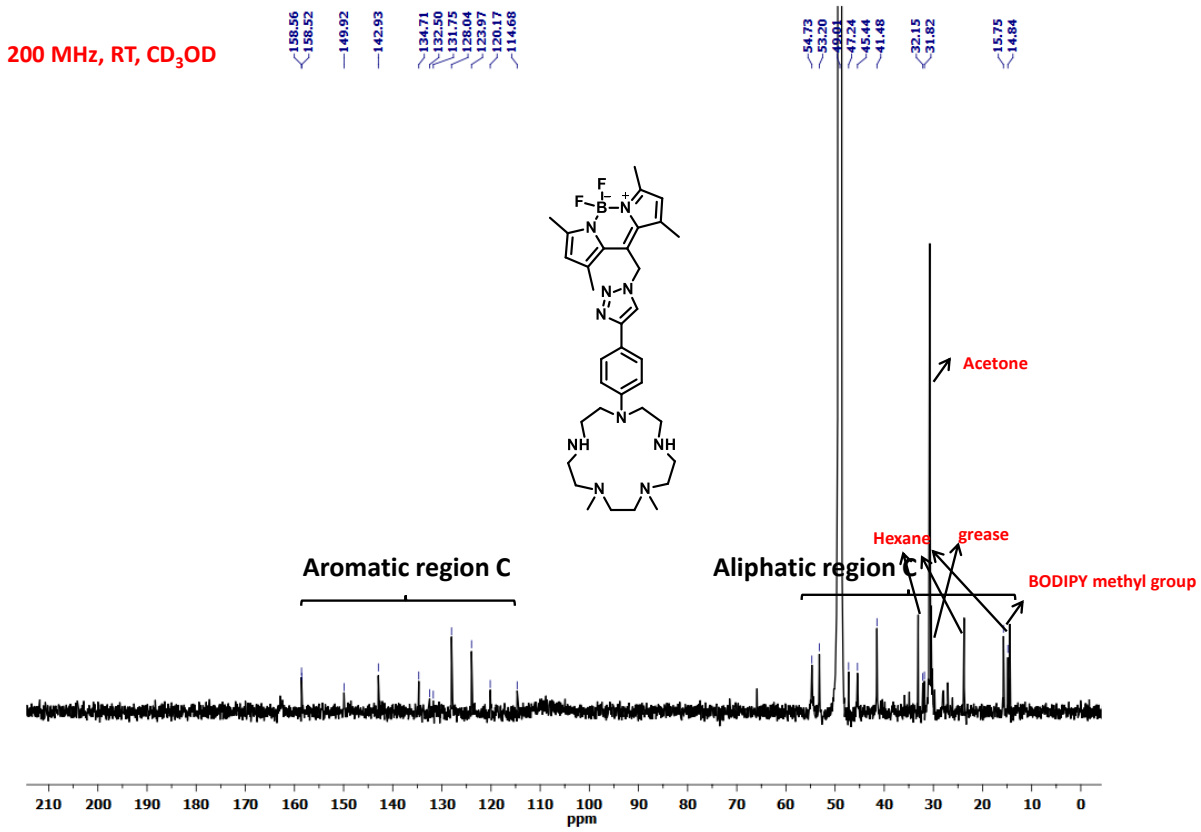

Figure S41. ^{13}C NMR spectrum of compound **M4**.

References

1. Monnereau, C.; Blart, E.; Odobel, F., A cheap and efficient method for selective para-iodination of aniline derivatives. *Tetrahedron Lett.* **2005,** *46* (32), 5421-5423.

2. Drew, M. E.; Chworos, A.; Oroudjev, E.; Hansma, H.; Yamakoshi, Y., A Tripod Molecular Tip for Single Molecule Ligand−Receptor Force Spectroscopy by AFM. *Langmuir* **2010,** *26* (10), 7117-7125.

3. Dapporto, P.; Formica, M.; Fusi, V.; Giorgi, L.; Micheloni, M.; Pontellini, R.; Paoli, P.; Rossi, P., Ligational Properties of Two New Phenolic Aza Cages towards Proton and Alkali Metal Ions − a Theoretical and an Experimental Approach. *Eur. J. Inorg. Chem.* **2001,** *2001* (7), 1763-1774.

4. Guo, B.; Peng, X.; Cui, A.; Wu, Y.; Tian, M.; Zhang, L.; Chen, X.; Gao, Y., Synthesis and spectral properties of new boron dipyrromethene dyes. *Dyes Pigm,* **2007,** *73* (2), 206-210.

5. Royzen, M.; Wilson, J. J.; Lippard, S. J., Physical and structural properties of [Cu(BOT1)Cl]Cl, a fluorescent imaging probe for HNO. *J Inorg. Biochem.* **2013,** *118*, 162-170.

6. Brannon, J. H.; Magde, D., Absolute quantum yield determination by thermal blooming. Fluorescein. *J. Phys. Chem.* **1978,** *82* (6), 705-709.